

Dear editor,

First, we would like to thank the two referees and the editor for dedicating their time to our manuscript and providing us with an in-depth feedback.

Our major revisions include the following points:

- We changed the title to “Continuous and autonomous snow water equivalent measurements by a cosmic ray sensor on an Alpine glacier”
- We improved (rewrote and rearranged several parts) the introduction by adding the points raised by referee #1, and by adjusting the story line.
- We improved the description of how we process the neutron count rate in Section 3.2 and additionally added a Section 3.4. This section includes an error propagation of the snow water equivalent derived by the cosmic ray sensor following the suggestions by referee #2. We also adapted Fig.2 accordingly and added an additional figure.
- We improved Fig.4 by changing its design (Fig.3 in first submission).
- Following the new estimation of the CRS precision, we adapted our evaluation of the daily changes in SWE and snow depth even though it did not change significantly (Table 6, Fig.7-8, in discussion part (Fig.6-7 and Table 4)
- We rewrote the discussion sections and split them into three sections:
 - Section 5.1 was re-structured and includes all the points raised by referee #1 and #2.
 - Section 5.3 was restructured in view of improving the story line of the paper.
- The conclusion was adapted to the points raised by referee #1 and #2.

Please find a point-by-point answer for each referee attached to this letter followed by all changes made in the original manuscript.

We hope to have addressed all major, moderate and minor concerns.

We thank you for considering the revised manuscript for publication, and look forward to hearing from you.

Rebecca Gugerli, on behalf of the authors

Author Response to Reviews of

Evaluating continuous and autonomous snow water equivalent measurements by a cosmic ray sensor on a Swiss glacier

Rebecca Gugerli, Nadine Salzmann, Matthias Huss and Darin Desilets
The Cryosphere Discussion, doi:10.5194/tc-2019-106

RC: *Reviewer Comment*, AR: *Author Response*, Manuscript text

Anonymous Referee #1

We would like to thank the anonymous referee #1 for his/her time and the thoughtful and constructive review, which significantly improves our manuscript.

Following the suggestions by referee #1 and #2, we decided to adapt the title of the paper to "Continuous and autonomous snow water equivalent measurements by a cosmic ray sensor on an Alpine glacier."

General comments

RC: *This paper presents the application of a sub-merged cosmic ray sensor (CRS) on a Swiss glacier to derive daily snow water equivalent (SWE) values for two winter seasons. An additionally installed snow depth (SD) sensor was used to calculate the snow density by CRS SWE and SD. For validation, some manual field measurements were conducted within the two years and precipitation recordings from nearby weather stations as well as a gridded precipitation product were scaled to compare them with the measured CRS SWE. The measurement results derived by CRS are very plausible for snow accumulation, densification and ablation phases. In general, this paper is well written and is, in my opinion, a good contribution to this journal. All measurements are well described and indicated by potential uncertainties and illustrated by significant figures. However, the main focus/ objective of this paper has to be better defined. Are you rather interested in gaining better snow density information or are you mainly focusing on using and validating CRS measurements especially on such a glacial test site, or both? Please emphasize on this – maybe also the title has to be changed accordingly. In some paragraphs, references should be added or revised. Below, I indicated some other moderate to minor issues.*

AR: *Thank you for your careful assessment and your constructive feedback. We have investigated the application of the cosmic ray sensor for measurements at a challenging site such as a glacier. The cosmic ray sensor (CRS) that lies below the snowpack has been presented in previous studies (e.g. Kodama, 1980, Paquet and Laval, 2005). A CRS which lies on a large hydrogen pool, such as ice, has been presented by (Howat et al., 2018) where they deployed a CRS on the Greenland ice sheet. To complement these studies, we assessed the application of this device on an Alpine glacier. The primary focus lies on the measurement setup and what new knowledge we gain from such observations. To state this more clearly, we rewrote the end of the introduction and state the study objective more clearly (see below).*

In this study, we investigate the applicability of a CRS installed below the snowpack to derive continuous SWE observations on an Alpine glacier in Switzerland (Glacier de la Plaine Morte). More specifically, we (i) analyse the CRS performance by comparing its SWE estimates to manual field observations. With the continuous observations of SWE and SD we (ii) analyze the evolution of snow density over the course of a winter season including the influence of meteorological conditions. Finally, we use the continuous observations to (iii) assess the performance of scaling readily available precipitation observations of nearby AWS and gridded precipitation data with a constant factor.

Specific comment

RC: *Please use the same units throughout the paper. SWE is usually given in mm (or kg/m²), not in cm w.e.*

AR: *We changed the units for snow water equivalent (SWE) to mm w.e., but kept the unit for snow depth (SD) as cm following the unit guidelines in Fierz et al. (2009). We adapted all figures accordingly.*

Abstract

RC: *p. 1, l 12-16: The aspect of the comparison of the cosmic ray SWE values and the scaled precipitation is represented quite dominant in the abstract. I think this aspect can be reduced to two 2 sentences and the abstract should better include also a statement on the general applicability.*

AR: *We agree and reduced it to two sentences.*

Moreover, we compare daily SWE amounts to precipitation sums from three nearby weather stations located at lower elevations, and to a gridded precipitation dataset. We determine the best-possible scaling factor for these precipitation estimates in order to reproduce the measured accumulation on the glacier. Using only one scaling factor for the whole time series, we find a mean absolute error of less than 8 cm w.e. for the reproduced snow accumulation. By applying temperature-specific scaling factors, this mean absolute error can be reduced to less than 6 cm w.e. for all stations. The continuous SWE measurements were also used to define a scaling factor for precipitation amounts from nearby meteorological stations. With this analysis, we show that a best-possible constant scaling factor results in cumulative precipitation amounts that differ by a mean absolute error of less than 80 mm w.e. from snow accumulation at this site.

1. Introduction

RC: *In general, a statement on remote sensing approaches to derive snow cover properties in alpine areas is missing (e.g. l. 31ff) – please give a short overview on such techniques.*

AR: *We included the following paragraph on remote sensing approaches.*

Spaceborne sensors can provide observations of snow cover, SWE and SD with a large spatial coverage. However, these observations often have a low spatial resolution and estimates of SWE are affected by snow properties such as the snow crystals and the liquid water content (Clifford, 2010, Dietz et al., 2012). In addition, uncertainties are increased for complex topographies (Smith and Bookhagen, 2016) and deep snowpacks (Smith and Bookhagen, 2018).

RC: *p.2, l.2: Not only the cold and windy conditions are a big challenge for in situ snow measurements in high mountains; please add that they are also often limited by difficult accessibility, complex terrain etc.*

AR: *We added a further sentence to explain the limited accessibility and complex terrain.*

MostlyIn particular, the cold and windy conditions pose the main challenge for accurate measurements (Sevruk et al., 2009, Rasmussen et al., 2012, Kinar and Pomeroy, 2015). The complex topography and limited accessibility add further challenges in high mountain regions.

RC: *p.2, l.13-21: The statements in this paragraph should be revised carefully as some statements are not correct. Some explanations are given in the following: Schmid et al. (2014) combined the upGPR with a snow depth sensor to additionally derive the liquid water content in snow. The main reasons for combining upGPR travel time with GPS signal strength in Schmid et al. (2015) were to eliminate an overestimation in snow depth during wet snow conditions, which would be the case by using only upGPR measurements, and to be independent of poles as both sensors were buried beneath the snowpack, which could be useful, e.g., in avalanche prone slopes. Moreover, with this upGPR-GPS sensor combination it was possible for the first time to derive SWE, snow height and liquid water content simultaneously. Schmid et al. (2015) is not suitable as reference in l.20 and Heilig et al. (2009) not for SWE measurements. Besides citing Steiner et al. (2018), Henkel et al. (2018, TGRS) and Koch et al. (2019, WRR) should be added as references in l.20. Besides snow accumulation, the GPS techniques derive snow properties under snow ablation/melt conditions. Additionally, in the latter reference, it was possible to derive three snow cover properties (SWE, snow depth and LWC) simultaneously with only one sensor setup.*

AR: *We revised this paragraph carefully, and changed it as follows.*

Ground-penetrating radar (GPR) is another method to determine snow accumulation and has been used in various studies (e.g. Heilig et al., 2009, 2010). Schmid et al. (2014) combine a snow depth (SD) sensor with an upward-looking GPR (upGPR) installed within the ground below the snowpack. This combination results in continuous estimates of liquid water content, SD and SWE at a high temporal resolution. SWE derived from this method lies within $\pm 5\%$ discrepancy from manual measurements. In a follow-up study, Schmid et al. (2015) combined an operational upGPR with a low-cost GPS to render the approach independent from additional sensors (e.g. SD). Despite the good agreement with manual measurements of SWE, the underlying algorithm to derive SWE from the upGPR is still prone to errors. For instance, a deviation of 10% in SD may lead to an over- or underestimation of 30-40% of the resulting SWE (Schmid et al., 2014). Furthermore, erroneous identifications of the reflection horizons affect the resulting SWE (Heilig et al., 2009; Schmid et al., 2015).

Other in situ devices include ground-penetrating radar (GPR) and sub-snow GPSs. Upward-looking GPR systems are installed below the snowpack and provide information about the snow stratigraphy (Heilig et al., 2009) and snow depth (SD, Heilig et al., 2010, Schmid et al., 2014). Combined with a low-cost GPS, Schmid et al. (2015) derived the liquid water content, SD and SWE independently from additional information and mast poles, making the system suitable for avalanche-prone slopes. Recent studies present sub-snow low-cost GPS as a promising method to continuously derive SWE (Steiner et al., 2018, Henkel et al., 2018, Steiner et al., 2019, Koch et al., 2019). This method uses two GPS antennas one of which is placed below and the other above the snowpack. Because the GPS signals are influenced when traveling through the snowpack, the difference in received signals can be used to quantify SWE, SD and liquid water content. GPS signals are freely available but the signal strength may be limited in high mountain regions depending on slope exposition and location (Koch et al., 2019).

RC: *p.3, l.23: I would not name it in a second application. This is rather a further type of validation (besides your manual SWE measurements) for CRS SWE.*

AR: *In general, we have more confidence in the SWE observations by the CRS than in the scaled precipitation measurements. For this reason, we use SWE to find the optimal scaling factor for precipitation and thereby assess an approach that has been previously applied.*

2. Study Site & 3. Data

RC: *I would suggest to merge sections 2 and 3.*

AR: *We added the section "Study site" under the Section "Data". In the revised manuscript, Section 2 is named "Study site and data".*

RC: *p.4, l.2: Although you have mentioned the altitude of your study site in the introduction, this should definitely also be mentioned in this section.*

AR: *We agree and modified the paragraph as follows.*

Our study site is located on the Glacier de la Plaine Morte (in the following: Plaine Morte) in Switzerland, where we deployed a subsurface CRS along with an ~~automatic weather station~~. This ~~glacier~~ AWS at an elevation of 2690 m a.s.l. (Fig. 1). Plaine Morte is situated on the ridge between ~~two Alpine regions of Switzerland~~, the Bernese Alps in the North and the Rhône valley in the South (Huss et al., 2013) ~~.Plaine Morte is particular in that it has almost no elevation gradient and is surrounded by mountain peaks with elevations from 2926 m.a.s.l (Pointe de la Plaine Morte) up to 3244 m a.s.l. (Wildstrubel, see Fig.1).~~

RC: *p.4, l.10f: How fast does the glacier move? Is there an effect on the measurements (e.g. on the SD sensor installed on a pole)?*

AR: *We added the following part to the section "Study site" to answer the question about the surface velocity. Concerning the second question, we did not add an explicit statement on this because we expect an effect of the glacier movement to be small. The AWS was designed not to be affected by glacier movement or ice melt. As shown in Fig.1d, it has three large wooden beams as a foundation of the main pole. We do address the influences of this mast design on the SD measurements in Section 5.2.*

[...] the winter snow distribution shows only a small spatial variability (Huss et al., 2013, GLAMOS, 2017)(GLAMOS, 2018) and the surface velocity is low (2-5 m per year according to Huss et al., 2013).

4. Methods

RC: *I would suggest including Subsection 4.1 in Section 3.*

AR: *We understand this point, but we decided against including subsection 4.1 into Section 3 because we consider it a method rather than data.*

RC: *The title of Subsection 4.2 might be misleading – it would be better to directly refer to CRS SWE and generally separate between SWE and snow density derivation.*

AR: *We split this section into two parts as suggested. In the revised manuscript the section names are as follows: 3.2 Calculating SWE from neutron counts, 3.3 Calculating snow density and daily changes in SWE, SD and snow density.*

RC: *p.7, l.26: Please insert a reference for the empirical parameters.*

AR: *The empirical function and its parameters have been provided by the manufacturer and previously used by Howat et al. (2018). We added this reference accordingly.*

RC: *p.8, Table 3: Not sure if it really makes sense and is sound to use for the gap filling different meteorological parameters from different stations (e.g. temperature from station a, humidity from station b etc.). In my opinion, rather one station with an overall best fit of all parameters should be used. Please state on this.*

AR: We understand this point of view. With regard to physical consistency and in, for example, an modeling application this aspect is crucial. In our study, however, we have independent SWE measurements which were not affected by the measurement gap of the station. To complete the bulk snow density evolution, we considered snow depth as the most important parameter and chose the best correlation for it (IMIS station SLFGA2). The correlation of temperature and relative humidity are similar for both, the chosen IMIS station (SLFDIA) and SLFGA2. For wind speeds, in contrast, the correlation is significantly smaller for SLFGA2 or SLFDIA compared to the chosen station (SLFGU2). In general, our results of the prevailing meteorological conditions during process-dominated days would remain similar. Figure 8a and b would remain similar because of the similar correlation. Figure 8d would also not be affected because wind is not displayed during the gap-period as we did not fill the data gap of wind direction.

RC: p.8, l.1: Please use just one unit for SWE (either mm or kg/m2). Regarding SD – in the figures, you use [cm] and here you define SD in [m] – this should be uniform throughout the paper.

AR: We adapted the units to mm w.e. for SWE and cm for SD following the guidelines suggested by Fierz et al. (2009). To make the equation consistent with the given units, we added a conversion constant (c) with a value 100 cm m^{-1} to the equation.

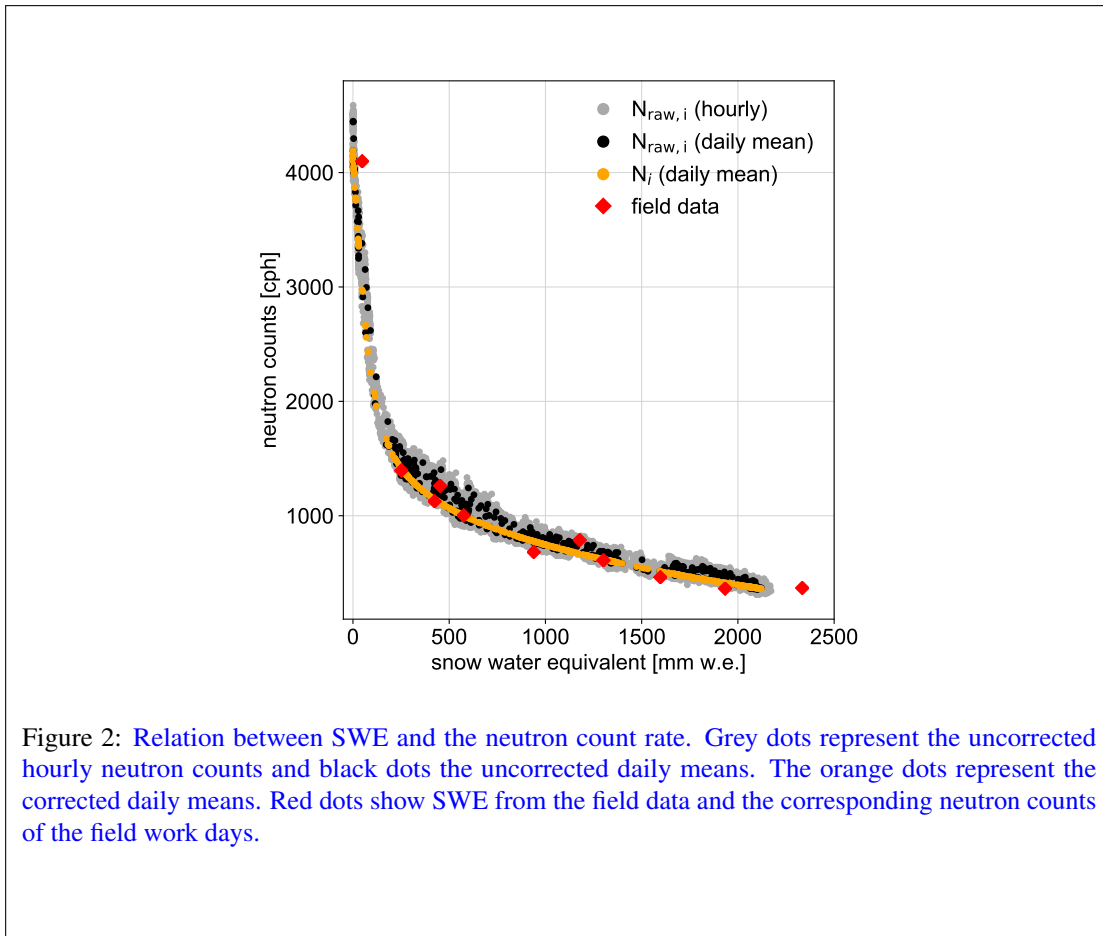
The bulk snow density ($\rho_{crs, sr} \rho_{crs_sr}$, in kg m^{-3}) is ~~then~~ derived from daily SWE (~~SWE_{crs} , in kg m^{-2}~~) (SWE_{crs} , in mm w.e. or kg m^{-2} , Fierz et al., 2009) and daily SD measurements (SD_{sr} , in ~~m~~cm) according to

$$\rho_{crs, sr} \rho_{crs_sr} = \frac{SWE_{crs}}{SD_{sr}} \cdot c \quad (1)$$

with c equal to 100 cm m^{-1} to assure unit consistency.

RC: p.9, Fig.2.a: Actually, no red or black crosses are visible in the figure (only red and grey horizontal lines) – please state on this and/or correct. Moreover, the error bars are not really readable. A revised version of this figure would be helpful (it could make sense to display the error bars in a separate figure).

AR: The crosses were not visible because the scale is too large for the uncertainties to be visible. We replaced Figure 2 with a new figure (see below). The uncertainties of SWE measurements are discussed and presented in a new section (Section 3.4 Estimating the uncertainty of CRS).



RC: *p.10, l.8: Please introduce N or do you mean N_i ?*

AR: *N refers to N_i . We corrected it throughout the manuscript.*

RC: *p.10, l.10: Why did you chose +/- 1cm? Can this be underlain with a reference?*

AR: *The systematic bias of +/- 1 cm originates from an analysis during snow free conditions (not shown), so it cannot be underlain with a reference. But we changed the uncertainty estimate of the SWE observations as suggested by referee #2 and documented it in Section 3.4 Estimating the uncertainty of the CRS. The new approach is based on error propagation of a non-linear equation and contains no additional systematic bias anymore.*

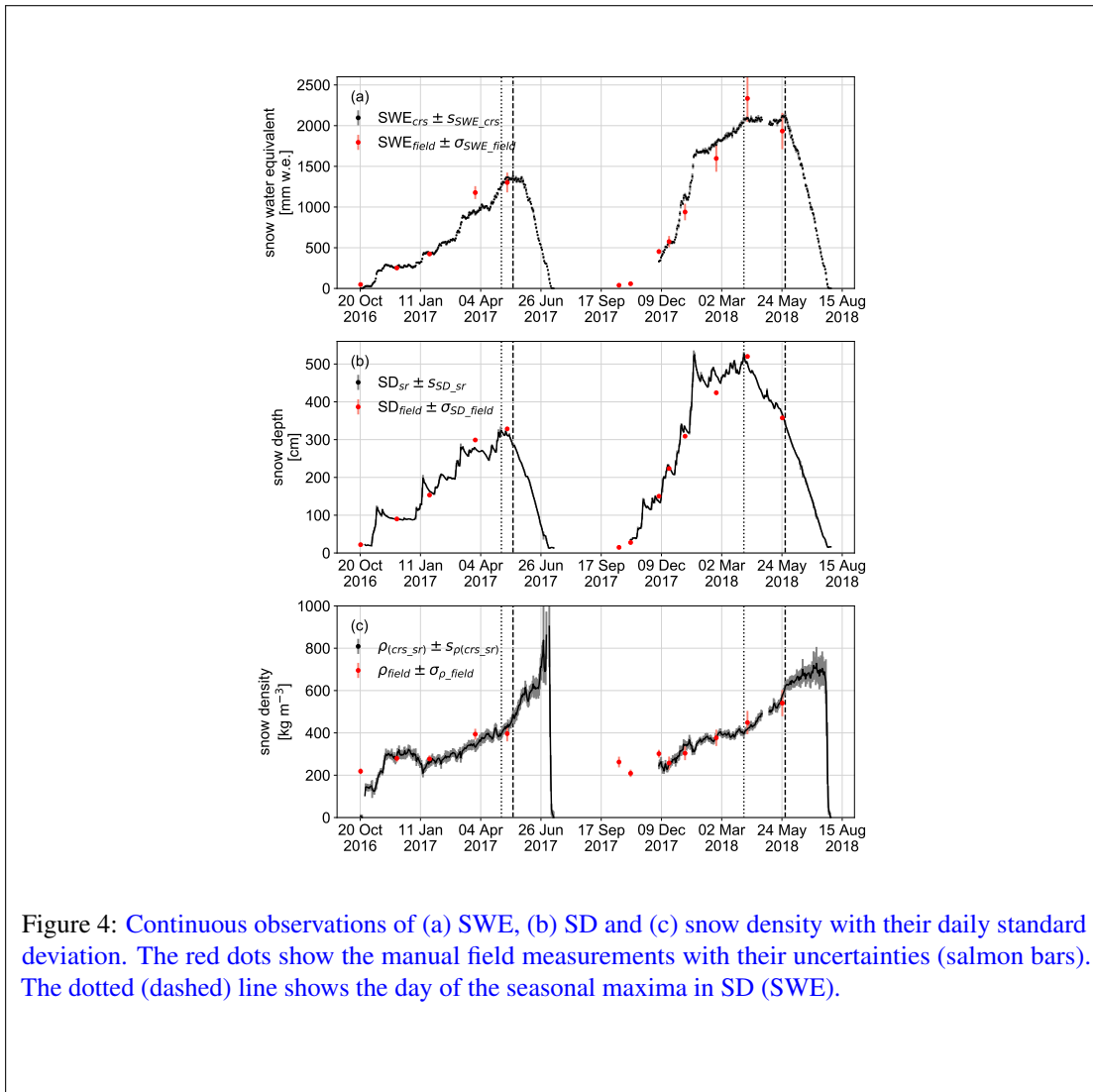
RC: *p. 10, l.19: In an earlier section you mentioned 4.8 m instead of 4.75 m – please unify.*

AR: *We changed it to 4.8 m consistently.*

5. Results

RC: *p.14, Fig.3: Please describe the vertical dashed lines in the figure caption or in a legend. In general, this figure would benefit to be displayed larger (if possible).*

AR: *We replaced this figure with an improved figure and adapted the figure caption (see below). In the revised manuscript, Figure 3 has become Figure 4.*



RC: *p.15, Fig.4: I really like this figure!*

AR: *Thank you.*

RC: *p.17, l.22: You should underlie the statement of rain gauge undercatch with a reference.*

AR: *In the revised manuscript, we added references for when we refer to undercatch by rain gauges. In the following, two relevant manuscript excerpts are shown.*

[Section 4.3.] Without applying a scaling factor, we see a large difference between cumulative precipitation and snow accumulation on the glacier (Fig. 9). This could be due to the high spatial variability of solid precipitation and/or undercatch of rain gauges (Kochendorfer et al., 2017, Pollock et al., 2018).

[Section 5.3] A drawback for AWS stations is the potentially large undercatch of solid precipitation combined with high wind speeds which can be on the order of a factor of three given solid precipitation and high wind speeds (Kochendorfer et al., 2017).

6. Discussion

RC: *Please add the following points in the discussion: Is there a general SWE limit by using CRS? How big is the footprint of the sensor and which shape does it have (e.g. conical)?*

AR: *For the general SWE limit no distinct value can be given because the relation between neutron counts and SWE is of an exponential nature. We added the following paragraph in Section 5.1 to address this point. To assess the footprint of a CRS lying below the snowpack is beyond the scope of this study. The dispersion and production of fast neutrons within the snowpack remains unclear and would require an in-depth investigation with a different study setup. Moreover, it probably would also require the modeling of neutron trajectories. In the new manuscript, we suggest an investigation on the footprint as a potential future study.*

In the second winter season, SWE amounts were exceptionally high with more than 2000 mm w.e. Nevertheless, the agreement to field measurement is within $\pm 10\%$ indicating that the measurement limit of SWE has not yet been reached. Due to the exponential nature of the relationship there is no distinct threshold beyond which the relative neutron count is no longer sensitive to SWE (Fig.2).

RC: *p.22, l.12: Please specify why there might be problems between 90 and 120 cm.*

AR: *We have removed this part from the manuscript because an explanation is too speculative. Moreover, we only apply the equation provided by the manufacturer. An investigation of further relations between neutron counts and SWE might help explain such discrepancies at these particular SWE amounts but is beyond the scope of this study. In general, our results show that the manual measurements are in good agreement with the given conversion equation (neutron counts - SWE, Fig.2). But, we discuss the potential influences of how we process raw neutron counts in the revised manuscript.*

RC: *p.22, l.26-30: Please insert references in this paragraph.*

AR: *We re-wrote the discussion on the CRS performance and limitations and rephrased this paragraph with reference to the introduction where all references are included.*

The main advantage of the CRS is that it can be deployed in an exceptionally wide variety of terrain. There is no need for a stable and flat surface nor does it depend on the reception of satellite signal for its measurements (cf. Section 1.1).

7. Conclusion

RC: *As this study investigates to a quite big extent the development of the snow density at your study site, this should also be mentioned more prominently in the conclusions section.*

AR: *We added the following paragraph in the conclusions.*

With the daily mean snow density observations, we showed that the evolution of the bulk snow density can be divided into three main periods; accumulation, densification and ablation. Throughout the accumulation period, snow densities are low with periodical repetitions of snowfall and subsequent densification. At the seasonal maximum of SWE the snowpack densifies during several days before its melting period begins. Additionally, we investigated these three processes at a daily basis and could attribute general meteorological conditions to each process.

Appendix A

RC: *In my opinion the appendix should be integrated in the methods section.*

AR: *We agree and integrated it in Section 3.2 Calculating SWE from neutron counts.*

RC: *p.25, l.12: Please introduce N also in the text.*

AR: *We dedicated a own section (3.2) on how we process neutron counts and adapted the variables accordingly.*

Author Response to Reviews of

Evaluating continuous and autonomous snow water equivalent measurements by a cosmic ray sensor on a Swiss glacier

Rebecca Gugerli, Nadine Salzmänn, Matthias Huss and Darin Desilets
The Cryosphere Discussion, doi:10.5194/tc-2019-106

RC: Reviewer Comment, **AR: Author Response,** Manuscript text

Anonymous Referee #2

We would like to thank the anonymous referee #2 for his/her time and the thoughtful and constructive review, which significantly improves our manuscript.

Following the suggestions by referee #1 and #2, we decided to change the title of the paper to "Continuous and autonomous snow water equivalent measurements by a cosmic ray sensor on an Alpine glacier".

General comments

RC: *This paper evaluates the snow accumulation on the Plaine Morte glacier by means of a buried cosmic-ray neutron probe (CRNS) and an approach based on the scaling of the precipitation records of nearby meteorological stations. The accuracy of the field data is assessed by the propagation of possible error sources. Together with the combined approach using different types of field data, this gives important insights into the evolution of the snow pack on the glacier. The language of the paper is appropriate, as are the figures and tables. Partly, the paper would benefit from considering a geographically broader view on the state-of-the-art as many references focus on Switzerland. In principle, the paper is suitable for publication in this journal. In particular, the added value of the paper lies in applying a buried CRNS together with other measurements for continuously monitoring the snow accumulation of a mountain glacier.*

AR: *Thank you for your valuable assessment and the interesting feedback. We admit that the state-of-the-art has many, but not only Swiss references. In the revised manuscript, we broadened the introduction and included more non-Swiss references.*

RC: *However, prior to further consideration for publication, the following two major concerns need to be addressed carefully:*

AR: *To address these two major concerns in more detail, we split the following comment of referee #2 into smaller parts. That allows us to directly address each raised point.*

RC: *(1) The story line of the paper needs to be clarified. The title and the final conclusions do not match well with the analysis made. Furthermore, the second part of the analysis is not (yet) connected to the rest of the paper. One could think of some logical links between the two parts, but it is important to state this more clearly, and to frame the rest of the paper accordingly. In addition, it would help the reader if the*

novelty would be more pronounced in the abstract and the conclusions.

AR: *The main focus of the paper is to assess the application of a cosmic ray sensor (CRS) in combination with the sonic ranging sensor for continuous snow water equivalent (SWE) and snow depth (SD) measurements on Alpine glaciers, and to show the advantages of such a measurement setup. We revised the story line of the paper and state our study objectives and the link between precipitation scaling and the CRS measurements more clearly.*

RC: *(2) While the error propagation of the snow depth, snow density and the meteorological measurements is reasonable and covers all important sources of uncertainty, this is not the case for the CRNS data. Most notably, the instrument's precision is most likely largely overestimated. Furthermore, a decrease of the error with increasing SWE is highly unlikely with mostly likely the opposite behavior being the case. Currently, only the uncertainty of the neutron count rate is considered, and a constant error is added despite the high non-linearity of the signal. The latter is probably the reason why the relative accuracy seems to increase with higher snow accumulation values. The statistical error of neutron count rate itself is an important element of measurement uncertainty, but it refers to uncorrected variations only. The uncorrected count rate includes variations not only of the accumulated SWE but also variations of incoming neutrons, atmospheric pressure, and in atmospheric moisture.*

AR: *We addressed this major concern in two ways. First, we approximate the precision by means of error propagation of a non-linear equation. Thereby, we take all corrections of the raw neutron count rate into consideration. With this approach, we also determine the driving uncertainty for the precision and present it in Figure 3b. The absolute precision decreases with increasing SWE. We calculated the precision for two temporal resolutions and show that the precision is considerably lower at the hourly resolution compared to the daily resolution. The calculation of the precision is documented in Section 3.4 of the revised manuscript and presented in the following.*

3.4 Estimating the uncertainty of the CRS

The calculated SWE is determined by the corrected neutron count relative to when the CRS is uncovered by snow ($N_{rel,i}$, Eq. 4). We base our error propagation on all corrections applied to the raw neutron count. Therefore, we assemble Eq.1-4 into

$$N_{rel,i} = N_{raw,i} \cdot \left(\beta \cdot \left(\frac{F_{inc,i}}{F_{inc,0}} - 1 \right) + 1 \right) \cdot \exp\left(\frac{p_i - p_0}{L}\right) \cdot \frac{1}{N_0} \quad (8)$$

The raw neutron count ($N_{raw,i}$), the incoming neutron flux ($F_{inc,i}$) and air pressure (p_i) change with time, but remain independent from each other. Following the rules of error propagation of a non-linear equation, we approximate the uncertainty in $N_{rel,i}$ as

$$\begin{aligned} \sigma_{N_{rel,i}}^2 \approx & \left(\frac{\partial N_{rel,i}}{\partial N_{raw,i}} \right)^2 \cdot \sigma_{N_{raw,i}}^2 + \left(\frac{\partial N_{rel,i}}{\partial N_0} \right)^2 \cdot \sigma_{N_0}^2 \\ & + \left(\frac{\partial N_{rel,i}}{\partial F_{inc,i}} \right)^2 \cdot \sigma_{F_{inc,i}}^2 + \left(\frac{\partial N_{rel,i}}{\partial F_{inc,0}} \right)^2 \cdot \sigma_{F_{inc,0}}^2 + \left(\frac{\partial N_{rel,i}}{\partial \beta} \right)^2 \cdot \sigma_{\beta}^2 \\ & + \left(\frac{\partial N_{rel,i}}{\partial p_i} \right)^2 \cdot \sigma_{p_i}^2 + \left(\frac{\partial N_{rel,i}}{\partial p_0} \right)^2 \cdot \sigma_{p_0}^2 + \left(\frac{\partial N_{rel,i}}{\partial L} \right)^2 \cdot \sigma_L^2 \quad (9) \end{aligned}$$

The uncertainty $\sigma_{N_{rel,i}}^2$ is then propagated through Eq.5 to estimate the uncertainty $\sigma_{crs,i}$

$$\sigma_{crs,i} \approx \sqrt{\left(\frac{\partial SWE_i}{\partial N_{rel,i}}\right)^2 \cdot \sigma_{N_{rel,i}}^2} \quad (10)$$

Since the uncertainties are not always known, we assume rather generous estimates for the uncertainties of all correction factors. Table 5 provides an overview of uncertainty estimates for all components.

For all neutron count rates ($N_{raw,i}$, N_0 , $F_{inc,0}$, $F_{inc,i}$), we assume poissonian counting statistics, which gives the uncertainty as the square root of the neutron counts (e.g. Zreda et al., 2012). With the integration over a time period t , the uncertainty is reduced by $t^{-0.5}$ (Schrön et al., 2018). While the relative uncertainty in $N_{raw,i}$ varies between 1.5%-5.3% for hourly observations, it varies between 0.3%-1% for the integrated daily estimates of our study.

The incoming radiation measured at Jungfraujoch has a low statistical uncertainty as its precision is high with around 190 counts per second. However, incoming radiation is corrected by an adjustment factor (β , Eq. 2) which is rather small for our site. Therefore, we assume also a small uncertainty of 0.03 for σ_β .

The uncertainty in air pressure (σ_{p_i} , σ_{p_0}) is based on the instrumental precision of 0.1 hPa (Lufft, 2019). For the mass attenuation length L , we use 132 hPa. An applied uncertainty of ± 2 hPa corresponds to the difference of shielding depths from latitudes north and south of Switzerland as shown in Fig.1 of Andreasen et al. (2017).

To render the error propagation more robust, we calculated $\sigma_{crs,i}$ using two different time resolutions. We additionally created a synthetic data set for both time resolutions. For the synthetic data set, we varied the time-dependent variables ($N_{raw,i}$, p_i , $F_{inc,i}$) uniformly within their observed minima and maxima values. At the hourly resolution it encompasses $4.8 \cdot 10^5$ hours and at the daily resolution it encompasses $4.8 \cdot 10^5$ days.

Figure 3a and b show the resulting precision for an hourly and daily resolution, respectively. Figure 3c and d show the relative contribution of every uncertainty term in Eq. 9, i.e. a high relative contribution indicates that the given parameter is an important source for the overall uncertainty of SWE. Figure 3 shows that the main uncertainty can be attributed to the neutron count uncertainty, independently of the time resolution. However, the precision estimate presented here does not include the uncertainty of the correction parameterization (Eq. 2 and Eq. 3) or the conversion equation (Eq. 5) and its parameters (Table. 4).

Table 5: Compilation of all direct observations and constants as well as the associated uncertainties σ at the hourly and daily scale. The units cph and cps stand for counts per hour and second, respectively. Brackets show the minimum and maximum within the time series.

Variables	hourly values	σ (hourly)	σ (daily)
$N_{\text{raw},i}$	[354; 4450] cph	$\sqrt{N_{\text{raw},i}}$ cph	$\sqrt{\frac{N_{\text{raw},i}}{24}}$ cph
N_0	4143 cph	64 cph	13 cph
$F_{\text{inc},i}$	[184; 195] cps	$\sqrt{\frac{F_{\text{inc},i}}{3600}}$ cps	$\sqrt{\frac{F_{\text{inc},i}}{86400}}$ cps
$F_{\text{inc},0}$	191 cps	0.2 cps	0.1 cps
β	0.95	0.03	0.03
p_i	[708; 747] hPa	0.1 hPa	0.1 hPa
p_0	739 hPa	0.1 hPa	0.1 hPa
L	132 hPa	2 hPa	2 hPa

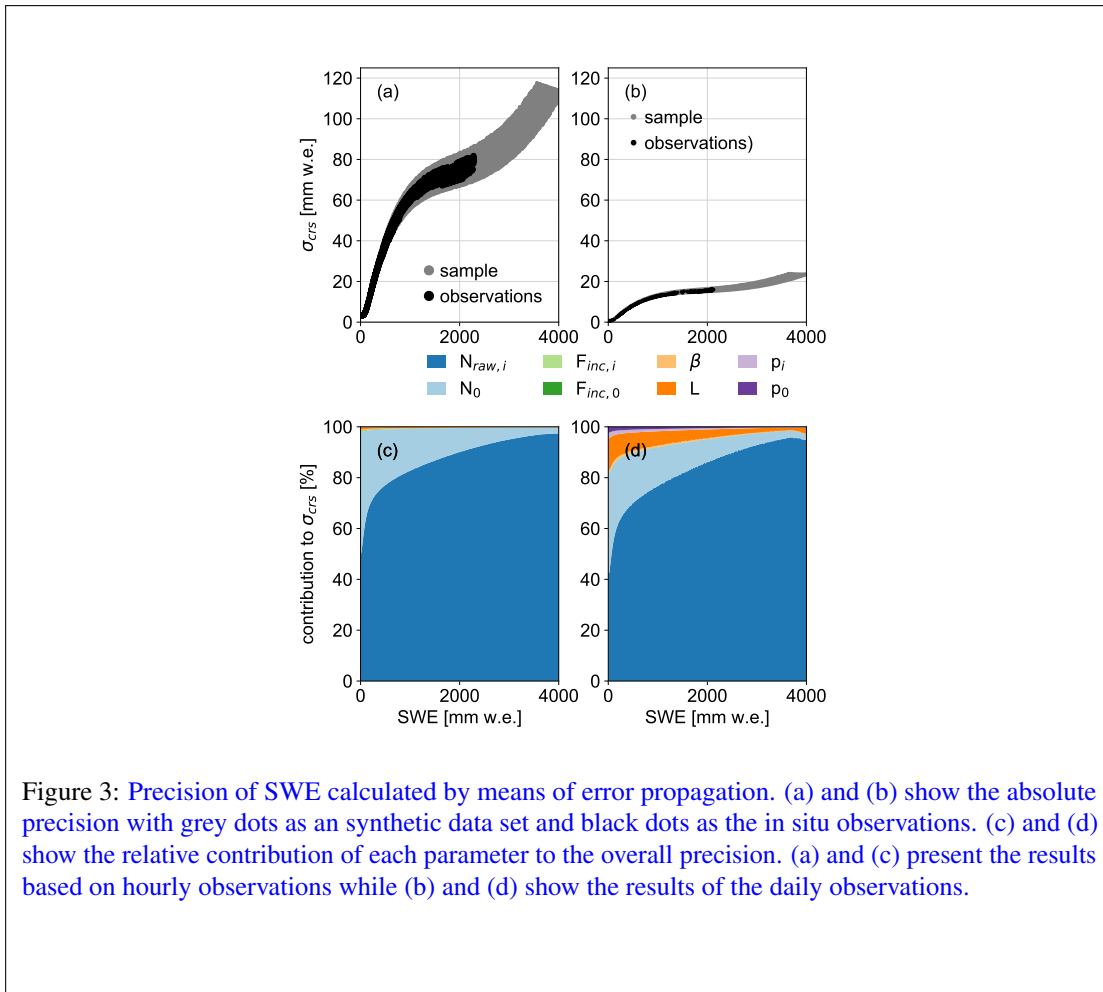


Figure 3: Precision of SWE calculated by means of error propagation. (a) and (b) show the absolute precision with grey dots as a synthetic data set and black dots as the in situ observations. (c) and (d) show the relative contribution of each parameter to the overall precision. (a) and (c) present the results based on hourly observations while (b) and (d) show the results of the daily observations.

RC: *An error propagation should thus include the uncertainty of (1) the neutron count uncertainty as already done, (2) the uncertainty of the measurements used for the corrections (Jungfraujoch neutron monitor data, atmospheric pressure, atmospheric moisture), (3) the uncertainty in the parameterisation of the correction functions (e.g., the value for the attenuation length, which may vary in space and time), and (4) the uncertainty in the (not well documented) empirical function relating neutron counts to SWE. In total, from figure 2 the error seems to be rather in the range of 10 to 20% (and thus around ten times larger than estimated in the paper!), with an increasing trend for high SWE values. Also the comparison with the manual measurements (figure 3) shows that the SWE from CRNS is mostly only touching the uncertainty bands of the manual measurements, while is partly entirely off.*

AR: *In the revised manuscript, we present an error propagation considering not only the neutron count uncertainty but also the uncertainty of the measurements used for the corrections. The uncertainty from the parameterisation of the correction function and the empirical function are not included in the calculations of Section 3.4 but clearly stated in this section and in the discussion. The relevant excerpt of the discussion section is shown in the following.*

5.1 CRS performance and limitations

The data processing of the neutron counts as presented is straightforward. Given the transformation equation, only the initial neutron count rate can be calibrated. But a variation of this calibration parameter within its uncertainties has little influence on the resulting SWE amounts, especially for amounts larger 400 mm w.e. This is a consequence of the exponential nature of the conversion equation (Eq. 5). More importantly, the neutron count rate may also be influenced by how we correct for air pressure and solar activity even though we apply the same equations as presented in previous studies for SWE (e.g. Howat et al., 2018) or soil moisture studies (e.g. Zreda et al., 2012, Andreasen et al., 2017). In contrast to previous studies of above-ground CRS, we do not correct for the changes in atmospheric moisture. We assume that for the below-ground CRS, fast neutrons are produced within the snowpack rather than in the atmosphere, an assumption also made in Howat et al. (2018), and implicitly made by preceding authors in their studies (e.g. Kodama et al., 1979, Paquet and Laval, 2005, Gottardi et al., 2013). Another source of uncertainty is the semi-empirical fit that has been used in this study. Because our study focuses on the application for snow and glacier studies, we have chosen to apply the relations used by Howat et al. (2018). In general, the conversion function has the potential to introduce considerable uncertainty in the inferred SWE. However, the applied empirical relation has shown to be adequate as the resulting SWE agrees well with independent field measurements, indicating only a minor bias and a standard deviation for individual observations that lie in the range of the uncertainty of the in situ SWE surveys.

For all correction factors such as air pressure and solar activity, we propagated an estimated uncertainty through all equations and show that the precision is mainly defined over the neutron count rate. Assuming that the parameterization of the correction equations carry no uncertainties, the influences of all other measurements and constant parameters are small. Moreover, an independent study by Howat et al. (2018) quantified a precision of 0.7% of a CRS lying below the snowpack on the ice sheet. Their results, however, are affected by lower in situ air pressure and consequently higher neutron count rate. In addition, Howat et al. (2018) observed lower SWE amounts which places them on a steeper part of the calibration curve (Fig. 2). For lower SWE amounts, changes in neutron counts are more sensitive and have a higher precision. The precision can be increased by integrating over longer time periods.

RC: *With the current focus of the paper the lack of a proper error propagation of the CRNS data constitutes a severe issue, as the evaluation and the precision of the CRNS are stated prominently in the title and conclusions. Still, it is interesting to see the application of CRNS for glacier monitoring and I agree with the authors that it constitutes a very promising technique for continuous accumulation measurements on glaciers. Existing uncertainties should, however, be kept in mind instead of propagating an unrealistically high precision of the SWE estimate. I believe there are two equally legitimate strategies on how the authors could address this. One is a true and rigorous error propagation with regard to all relevant uncertainty sources of the CRNS SWE estimate. Another could lie in drawing the reader's attention to the fact, that the uncertainty range could be substantially (up to ten times) larger, combined with reframing the paper towards the application rather than the error propagation.*

AR: *We addressed the major concern of referee#2 in two different ways. First, we calculated a precision based on the neutron count rate and the correction measurements. Second, we draw the readers attention to all uncertainties related to the processing of the raw neutron count in the discussion. Since the main focus of the paper is the application of a CRS, an in-depth investigation of the uncertainties in the correction parameterizations and the semi-empirical conversion equation would be beyond the scope of this study. We adjusted the title and story line of the paper accordingly.*

Specific comment

RC: *Page 3/ Line 33-34: Check the sentence ("..define three different scaling factors, one for...“?).*

AR: *This part was rewritten and does not include the specific sentence anymore.*

RC: *Page 4/ Line 2: It would be helpful when the elevation of the glacier and the surrounding mountain peaks would be added here.*

AR: *We modified the beginning of Section 2.1 Study site as follows.*

Our study site is located on the Glacier de la Plaine Morte (in the following: Plaine Morte) in Switzerland, where we deployed a subsurface CRS along with an ~~automatic weather station. This glacier-AWS~~ at an elevation of 2690 m a.s.l. (Fig. 1). Plaine Morte is situated on the ridge between ~~two Alpine regions of Switzerland~~, the Bernese Alps in the North and the Rhône valley in the South (Huss et al., 2013). ~~Plaine Morte is particular in that it has almost no elevation gradient.~~ and is surrounded by mountain peaks with elevations from 2926 m.a.s.l (Pointe de la Plaine Morte) up to 3244 m a.s.l. (Wildstrubel, see Fig. 1). With a surface area of 7.4 km² ~~it~~ and a particularly low elevation gradient, Plaine Morte is the largest plateau glacier in the European Alps. ~~Due to its flatness~~ Most of its surface is located between 2650 m a.s.l. and 2800 m a.s.l. (GLAMOS, 2018).

RC: *Page 5/ Line 18: Can you add a few key facts on how the gridded products is produced. Does it contain station data? If so, how reliable is it when the nearby stations have data gaps?*

AR: *We added the following paragraph to Section 2.2.*

The gridded precipitation product, RhiresD, uses rain-gauge measurements from around 400 automatic as well as manual observations. These observations (not available in real time) are quality-checked prior to their processing. The observations are spatially analysed, pre-processed and interpolated to a 1 × 1 km grid at daily resolution covering the Swiss territory (MeteoSwiss, 2013). The main sources of uncertainty arise from the interpolation, the rain-gauge measurements, the grid spacing and its effective resolution, and the temporal variation of the number of stations. For further information, the reader is referred to the technical document provided by MeteoSwiss (MeteoSwiss, 2013). We extracted daily precipitation estimates of the three grid points closest to the position of the CRS (Table 2 and Fig. 1c).

RC: *Page 6/ Table 2: Think of readers that are not familiar with the Swiss coordinate system. I would recommend converting the station coordinates into a globally used system like UTM or WGS84 (lat/lon). In any case, add also the EPSG-code of the coordinate system.*

AR: *We added the WGS84 coordinates of the AWS and the RhiresD in the corresponding table. For RhiresD, we kept the Swiss coordinates to help the reader find the grid cells in Fig.1c. Additionally, we added a cross in the lower left corner of Fig.1c with the corresponding WGS84 coordinates.*

RC: *Page 7 Line 1: The reliability of the CRNS is one of the objectives, thus could not be claimed beforehand.*

AR: *We changed the paragraph as follows.*

~~Once deployed, the CRS measured reliably. The CRS, in contrast, measured continuously over the two winter seasons with one exception. During the exception of a short period end of April 2018, the CRS measured irregularly because of a problem with the connector. However, after fixing a faulty connection, the CRS then continued measuring without our interference. In summer 2018, we changed the connector and measurements have been without gaps since. need for further maintenance.~~

RC: *Page 23/ Line 2: the effect is related to SWE not to density.*

AR: *We split the discussion section into two parts and rewrote both which changed also this sentence.*

RC: *Page 23/ Line 8: Here, too much confidence is set into CRNS.*

AR: *We rewrote this section and state all influences of snow density estimates more clearly. In the following the corresponding revised paragraph of the manuscript is presented.*

[...] The high snow densities presented here could be a result of changes in the snow physics, measurement errors of SWE and SD estimations (Eq. 7), or a combination of both. Physical changes within the snowpack could be due to refreezing of liquid water at several layers within the snowpack, water saturated snow in the top layers, locally thick ice lenses, or accumulation of liquid water around the CRS which eventually refreezes. ~~With the CRS and the SR, we can only determine a mean snow density. Therefore, not all these effects would be identifiable, and explanations remain speculative. Despite all potential explanation for errors by the CRS, it could also be a problem with the SD measurements rather than the SWE measurements. In our study setup, several reasons could cause erroneous SD measurements. Firstly~~ SWE from the CRS could, for example, be affected by a suprafacial pond in the vicinity of the site. It remains unclear how such a hydrogen pool would influence the in situ point measurements of the below-ground CRS. Other influences could come from the correction factors of the neutron count rate or the conversion equation applied in this study (cf. Section 5.1). The SD measurements are also susceptible to errors. For example, the snow area below the sonic ranging sensor may show a small depression because of wind turbulence caused by the mast. ~~Furthermore~~ Additionally, the snow around the ~~metal mast~~ main pole of the station melts faster possibly leading to a depression ~~with a larger radius around the mast~~. It remains difficult to assess whether the radius of this depression would be within the footprint of the sonic ranging sensor. ~~Nevertheless, these two effects may superimpose. Secondly~~ In winter 2017/18, the solar panels were submerged below the snow. To ensure further power supply, we had to ~~free the solar panels by digging a dig~~ them out. This snow pit around the ~~mast in winter 2017/18. This snow pit~~ main pole would have been refilled by wind, but densities are different, probably causing accelerated melt rates around the mast. ~~Thirdly, the influences~~ For more shallow snowpacks, the metal anchorage of the mast's foundations, ~~the wooden beams with the metal anchorage, may cause erroneous SD measurements for more shallow snowpacks. This also becomes clear since SD measurements never reach~~ might interfere with the SD measurements. The SD measurements, for instance, never observe a SD of 0 cm even though the sensor is calibrated for the mounted height and agreements to snow probes agree during the season (Fig. 4) ~~-b and Fig. 6).~~

To underline this statement, we show a photo from the mast taken in June 2019. We did not include this photo

in the revised manuscript. Between the last field work in April 2019 and this one, the site was not visited, and we encountered it with the large depression around the mast itself.



Figure 4: Photo of the mast installation taken in June 2019.

Evaluating ~~continuous~~ Continuous and autonomous snow water equivalent measurements by a cosmic ray sensor on ~~a Swiss an~~ Alpine glacier

Rebecca Gugerli¹, Nadine Salzmann¹, Matthias Huss^{1,2}, and Darin Desilets³

¹Department of Geosciences, University of Fribourg, Fribourg, Switzerland

²Laboratory of Hydraulics, Hydrology and Glaciology (VAW), ETH Zurich, Zurich, Switzerland

³Hydroinnova LLC, Albuquerque, NM, USA

Correspondence: Rebecca Gugerli (rebecca.gugerli@unifr.ch)

Abstract. Snow water equivalent (SWE) measurements of seasonal snowpack are crucial in many research fields. Yet accurate measurements at a high temporal resolution are difficult to obtain in high mountain regions. With a cosmic ray sensor (CRS), SWE can be directly derived ~~inferred~~ from neutron counts. ~~In this study, we~~ We present the analyses of temporally continuous SWE measurements by a CRS on ~~a Swiss glacier an~~ Alpine glacier in Switzerland (Glacier de la Plaine Morte) over two winter seasons (2016/17 and 2017/18), which ~~were markedly different in terms of~~ differed markedly in the amount and timing of snow accumulation. By combining ~~the SWE values~~ SWE with snow depth measurements, we calculate the daily mean density of the snowpack. ~~The~~ Compared to manual field observations from snow pits the autonomous measurements overestimate SWE by ~~+2%±12% compared to manual field observations (snow pits)~~ 13%. Snow depth and ~~mean density agree with manual in-situ measurements with a standard deviation of the bulk snow density deviate from the manual measurements by~~ ±6% and ±8%, ~~respectively. In general, the cosmic ray sensor has~~ 9% respectively. The CRS measured with high reliability ~~during these over~~ two winter seasons and is ~~, thus, considered an effective method to measure~~ thus considered a promising method to observe SWE at remote ~~high~~ high-alpine sites. We use the daily observations to ~~break down the winter season into days either~~ classify winter season days into those dominated by accumulation (solid precipitation, ~~wind-snow~~ wind-snow drift), ablation (~~wind-snow~~ wind-snow drift, melt) or snow densification. ~~The~~ For each of these process-dominated days the prevailing meteorological conditions ~~of these periods are~~ clearly distinct for each of the classified processes. Moreover, we compare daily SWE amounts to precipitation sums from three ~~nearby weather stations located at lower elevations, and to a gridded precipitation dataset. We determine the~~ are distinct. The ~~continuous SWE measurements were also used to define a scaling factor for precipitation amounts from nearby meteorological stations. With this analysis, we show that a~~ best-possible ~~scaling factor for these precipitation estimates in order to reproduce the measured accumulation on the glacier. Using only one scaling factor for the whole time series, we find~~ constant scaling ~~factor results in cumulative precipitation amounts that differ by~~ a mean absolute error of less than ~~8 cm~~ 80 mm w.e. ~~for the reproduced snow accumulation. By applying temperature-specific scaling factors, this mean absolute error can be reduced to less than 6 cm w.e. for all stations. from snow accumulation at this site. The annual amount of~~

1 Introduction

The evolution and amount of the seasonal snow accumulation in high mountain regions is a key parameter in many climate-related research fields such as glaciology or hydrology and climate change impacts, risks and adaptation. Changes in snow accumulation in mountain areas caused by climate change are expected to have major impacts on water supply for adjacent lowlands (Barnett et al., 2005; Viviroli et al., 2007, 2011), hydropower production (Ali et al., 2018) or winter tourism (Marty et al., 2014; Sturm et al., 2017). In addition, information of the amount of water stored within the annual snowpack (snow water equivalent, SWE) in high mountain regions is crucial for avalanche ~~prediction~~-warning (Castebrunet et al., 2014), flood prevention (Jörg-Hess et al., 2015), or mass balance calculations of glaciers (Sold et al., 2013; Pulwinski et al., 2018). Despite the high demand for accurate SWE measurements in high mountain regions, reliable and temporally continuous measurements of SWE are still difficult to obtain. ~~Mostly~~In particular, the cold and windy conditions pose the main challenge for accurate measurements (Sevruk et al., 2009; Rasmussen et al., 2012; Kinar and Pomeroy, 2015). The complex topography and limited accessibility add further challenges in high mountain regions.

~~Manual in-situ~~In this study we focus on providing temporally continuous and autonomous observations of SWE in glacierized high mountain regions to improve our understanding of the seasonal evolution of the snowpack.

1.1 State-of-the-art snow accumulation observations

A wide range of different devices are used to measure snow accumulation (Kinar and Pomeroy, 2015; Pirazzini et al., 2018), each with its advantages and clear tradeoffs. Manual in situ field measurements with snow pits and snow probes ~~usually can~~ provide reliable data ~~. Nevertheless, they are not suited for continuous measurements because they are but have a low temporal resolution. Such measurements are also~~ invasive, laborious, and logistically complicated for remote sites. ~~Various devices to measure snow accumulation autonomously and continuously at high elevations have been tested and applied during the past decades (Pirazzini et al., 2018)~~

According to Pirazzini et al. (2018) snow gauges, a rain-gauge adapted for solid precipitation, are often used in Europe. However, the uncertainty of these devices remains high. For example, snow gauges they are known to carry large uncertainties in the extreme environments of high mountains through undercatch and post-event thawing (e.g. Goodison et al., 1998; Rasmussen et al., 2001). ~~Snow pillows (e.g. Goodison et al., 1998; Rasmussen et al., 2012; Martinaitis et al., 2015; Pollock et al., 2018). Current instruments relying on the mass or pressure of overlying snow (e.g. snow pillows and snow scales) are rarely suitable in not well suited for high mountain regions because they require a large flat surface (e.g. Egli et al., 2009; Kinar and Pomeroy, 2015). In addition, ice bridging can falsify the measurements (e.g. Sorteberg et al., 2001; Johnson and Schaefer, 2002). Ground-penetrating produce large errors (e.g. Sorteberg et al., 2001; Johnson and Schaefer, 2002).~~

Other in situ devices include ground-penetrating radar (GPR) is another method to determine snow accumulation and has been used in various studies (e.g. Heilig et al., 2009, 2010). Schmid et al. (2014) combine a snow depth (SD) sensor with an upward-looking GPR (upGPR) installed within the ground and sub-snow GPSs. Upward-looking GPR systems are installed below the snowpack . This combination results in continuous estimates of and provide information about the snow stratigraphy

(Heilig et al., 2009) and snow depth (SD, Heilig et al., 2010; Schmid et al., 2014). Combined with a low-cost GPS, Schmid et al. (2015) derived the liquid water content, SD and SWE at a high temporal resolution. SWE derived from this method lies within $\pm 5\%$ discrepancy from manual measurements. In a follow-up study, Schmid et al. (2015) combined an operational upGPR with a independently from additional information and mast poles, making the system suitable for avalanche-prone slopes. Recent studies present sub-snow low-cost GPS to render the approach independent from additional sensors (e.g. SD). Despite the good agreement with manual measurements of SWE, the underlying algorithm to derive SWE from the upGPR is still prone to errors. For instance, a deviation of 10% in SD may lead to an over- or underestimation of 30-40% of the resulting SWE (Schmid et al., 2014). Furthermore, erroneous identifications of the reflection horizons affect the resulting SWE (Heilig et al., 2009; Schmid et al., 2015). Steiner et al. (2018) present sub-snow GPS as a method to continuously monitor snow accumulation. Data processing of the GPS signals is elaborate as a promising method to continuously derive SWE (Steiner et al., 2018; Henkel et al., 2018; Steiner et al., 2019; Koch et al., 2019). This method uses two GPS antennas one of which is placed below and the other above the snowpack. Because the GPS signals are influenced when traveling through the snowpack, the difference in received signals can be used to quantify SWE, SD and liquid water content. GPS signals are freely available but the signal strength may be limited in high mountain regions depending on slope exposition and location (Koch et al., 2019).

Spaceborne sensors can provide observations of snow cover, SWE and SD with a large spatial coverage. However, these observations often have a low spatial resolution and estimates of SWE are affected by snow properties such as the snow crystals and the liquid water content (Clifford, 2010; Dietz et al., 2012). In addition, uncertainties are increased for complex topographies (Smith and Bookhagen, 2016) and deep snowpacks (Smith and Bookhagen, 2018).

Other approaches use empirically derived or physically calculated bulk snow densities to calculate the SWE with additional meteorological parameters to calculate SWE from continuous SD measurements. The approach presented by Jonas et al. (2009), for instance, uses automatic measurements of SD with an empirically derived model to estimate the SWE. Empirical models often estimate a bulk snow density in various regions of the Swiss Alps for different elevations and months. The model agreement to manual measurements lies within the site variability of snow density and SWE. However, the model performance is limited with its temporal resolution. A model that allows the calculation of SWE if combined with SD data (e.g. Jonas et al., 2009; Sturm et al., 2010). More recently, Hill et al. (2019) proposed an empirical model to derive SWE from SD measurements in regions where no automatic weather station (AWS) data is available. For avalanche forecasting operational models are usually physically-based model in operational use is, for instance, the model SNOWPACK (Lehning et al., 1999). The Swiss Federal Institute for Snow and Avalanche Research combines this model with meteorological parameters measured at high-elevation automatic weather stations to derive snow properties for avalanche forecasting (Lehning et al., 1999). In general, Raleigh and Small (2017) show that 75% of the uncertainty of estimated SWE is caused by the uncertainty of modeled snow density. In their study, they observed SD with an airborne lidar and modeled snow density with four different models (two empirically based and two physically based) (e.g. Crocus, Vionnet et al., 2012, SNOWPACK, Lehning et al., 1999) and require high-quality meteorological data to derive accurate snow properties. Such model-based approaches are sensitive to errors in the input data. For example, erroneous precipitation observations (Raleigh et al., 2015) and/or uncertainties in modeled snow density may influence the results significantly (Raleigh and Small, 2017).

A simplified approach utilizes precipitation observations from nearby AWS and accounts for the bias in cumulative seasonal precipitation through use of a temporally constant scaling factor derived from on-glacier point SWE measurements at the end of winter. This approach is used for the operational evaluation of the winter mass balance on Swiss glaciers (GLAMOS, 2018) where seasonal manual measurement of SWE are combined with readily available precipitation data. Despite the heterogeneity of precipitation and the influence of preferential deposition and snow drift, the simplified approach has provided reasonable results for the purpose of glacier mass balance observations (see e.g. Huss et al., 2009, 2015; Sold et al., 2016).

1.2 Cosmic ray sensor

The cosmic ray sensor (CRS) is a ~~re-discovered method device~~ to measure snow accumulation ~~continuously~~, temporally continuous. The method relies on the attenuation of natural radiation by snow. A CRS counts the number of fast neutrons ~~, which originate from the interaction of cosmic rays with various nuclei within the Earth's atmosphere. When these neutrons arrive at the Earth's surface, hydrogen atoms easily moderated them. Thus, the number of neutrons and the one used in this study is installed at ground level, and is allowed to get buried by snow. On the surface of a glacier, most of the fast neutrons originate from the atmosphere and are moderated by the hydrogen atoms contained in water (whether in solid or liquid form). Hence, the neutron counting rate~~ is negatively correlated to the number of hydrogen atoms ~~present in the vicinity and allow inferring the SWE (Zreda et al., 2008; Desilets et al., 2010). The CRS has first been above the sensor. A CRS was~~ deployed by Kodama et al. (1975) and Kodama (1980) in the ~~70s and already 1970s and~~ showed promising results with an error of less than 7% for cosmic-ray-derived SWE measurements compared to manual measurements. Almost 20 years later, the ~~French Electric Utility Électricité de France~~ developed their own CRS and integrated these in a mountain monitoring network in order to manage hydroelectric power (Paquet and Laval, 2005; Paquet et al., 2008). In 2013, this monitoring network counted 37 sites in the French Alps and the Pyrenees (Gottardi et al., 2013). ~~These CRS are all installed below the snowpack. More recent~~ Recent studies have investigated the potential of SWE measurements with ~~above-ground CRS, which CRS installed above the snowpack. These~~ provide a larger footprint ~~of 230-300 m with a radius on the order of tens to hundreds of meters~~ (Sigouin and Si, 2016; Schattan et al., 2017). Independently of the sensor's deployment above or below the snowpack, the SWE measurements ~~were are known to be~~ influenced by changes in soil moisture through snow melt (Kodama, 1980; Paquet and Laval, 2005; Sigouin and Si, 2016). A shield was thus added to the ~~invasive~~ CRS to prevent influences from increases in soil moisture from the surrounding ground (Paquet and Laval, 2005). Schattan et al. (2017) state that ~~this with the non-invasive sensor the~~ effect is negligible for ~~deeper snowpack's. Nevertheless, these influences can be almost entirely deep snowpacks. These influences are~~ avoided by placing the CRS on an ice surface such as a polar ice sheet or a mountain glacier. In the recent study by Howat et al. (2018), the CRS was deployed below the snowpack on the Greenland Ice Sheet. With almost 24 months of measurements, they find an instrument precision of approximately 0.7% and a good agreement with manual measurements.

1.3 Study objectives

In this study, we ~~evaluate investigate~~ the applicability of ~~the CRS for continuous SWE measurement on a CRS installed below the snowpack to derive continuous SWE observations on an Alpine glacier in Switzerland (Glacier de la Plaine Morte in the~~

Swiss Alps, including a rigorous uncertainty analysis. On the given glacier site (2690 masl), we have a generally lower neutron counts than in the study by Howat et al. (2018) which is at 3216 masl. This is due to the lower latitude and elevation. Moreover, the combination with continuous SD measurements allows the calculation of the bulk snow density at a daily resolution. With the daily density values, we analyze the temporal evolution of the bulk ~~SD~~. More specifically, we (i) analyse the CRS performance by comparing its SWE estimates to manual field observations. With the continuous observations of SWE and SD we (ii) analyze the evolution of snow density over two winter seasons. Furthermore, we analyse the general processes within the snowpack by applying criteria to daily changes in SD and SWE. Thereby, we identify the days that are dominated by accumulation, ablation, and densification. For each of these process-classified days we investigate their prevailing ~~SD~~ the course of a winter season including the influence of meteorological conditions.

In a second application, we aim at reproducing snow accumulation by using precipitation estimates from nearby stations at lower elevations. Because estimates of precipitation that are automatic and continuous are even more challenging to obtain in high mountain regions, considerable uncertainties are introduced in many mountain precipitation climatologies (e.g. Efthymiadis et al., 2009). Nonetheless, such precipitation data is useful. One useful application is, for example, the operational evaluation of winter mass balance on Swiss glaciers (GLAMOS, 1881-2018). Based on scaling daily precipitation to observed end-of-season measurements of SWE, the temporal evolution of mass balance is inferred (see e.g. Huss et al., 2009, 2015; Sold et al., 2016). In the case of Plaine Morte and its mass balance monitoring, for instance, precipitation amounts are currently taken from the Montana weather station, which is in the vicinity of the glacier (Huss et al., 2013; GLAMOS, 1881-2018). Given the continuous observations of SWE, we evaluate the application of a constant scaling factor on the precipitation observations to reproduce snow accumulation on the glacier. In a simple approach, we use only one scaling factor on a selection of weather stations. Finally, we use the continuous observations to (iii) assess the performance of scaling readily available precipitation observations of nearby AWS and gridded precipitation data. In a more elaborate approach, we define three different scaling factors for each weather stations. The three scaling factors depend on the hourly air temperature on the glacier. with a temporally constant factor.

2 Study site and data

2.1 Study site

Our study site is located on the Glacier de la Plaine Morte (in the following: Plaine Morte) in Switzerland, where we deployed a subsurface CRS along with an automatic weather station. This glacier AWS at an elevation of 2690 m a.s.l. (Fig. 1). Plaine Morte is situated on the ridge between two Alpine regions of Switzerland, the Bernese Alps in the North and the Rhône valley in the South (Huss et al., 2013).

Plaine Morte is particular in that it has almost no elevation gradient and is surrounded by mountain peaks with elevations from 2926 m a.s.l (Pointe de la Plaine Morte) up to 3244 m a.s.l. (Wildstrubel, see Fig. 1).

With a surface area of 7.4 km² it and a particularly low elevation gradient, Plaine Morte is the largest plateau glacier in the European Alps. Due to its flatness, Most of its surface is located between 2650 m a.s.l. and 2800 m a.s.l. (GLAMOS, 2018). Due

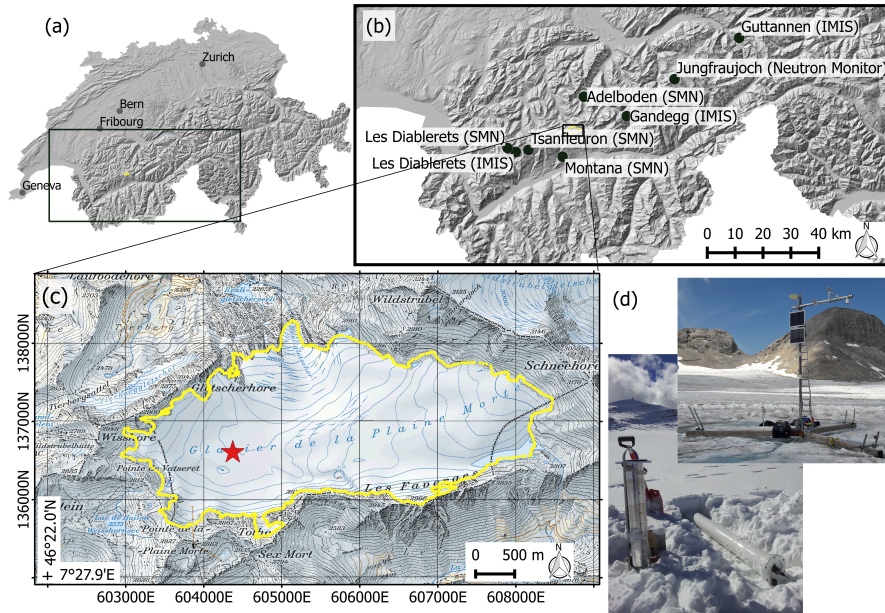


Figure 1. (a) Map of Switzerland. (b) Map of the excerpt marked in (a), and all weather stations used in this study (black dots). (c) Topographic map of Plaine Morte with the red star indicating the location of the AWS with the CRS (see (d), [46°22.8'N, 7°29.7'E](#)). The yellow contour represents the current outline of Plaine Morte (Fischer et al., 2014). The coordinates correspond to the Swiss coordinate system ([CH1903EPSG: 21781](#)). (Maps provided by Swisstopo).

to lack of elevation gradient, the equilibrium line ~~is can be~~ located either above or below the glacier surface, rendering it ~~either~~ completely snow-free or snow-covered at the end of summer, ~~respectively~~. For the same reason, the winter snow distribution shows only a small spatial variability ([Huss et al., 2013](#); [GLAMOS, 2017](#)) ([GLAMOS, 2018](#)) and the surface velocity is low ([2-5 m per year according to Huss et al., 2013](#)).

- 5 Since its ~~integration inclusion~~ in the glacier monitoring network of Switzerland ~~in 2009~~, the annual ~~mass balance glacier-wide~~ mass balance for the hydrological years between 2009 and 2019 has been negative with an average loss of ~~1.4 m~~ 1477 mm w.e. ~~per year. This is despite a mean winter gain between 2009 and 2017 of 1.3±0.2 m~~ Average glacier-wide winter mass balance was 1338 mm w.e. ~~between 2010 and 2019~~ (GLAMOS, 1881-2018).

3 Data

- 10 In October 2016, we installed an ~~automatic weather station~~ AWS on Plaine Morte ([46° 22.8' N, 7°29.7' E](#), 2690 ~~maslm a.s.l.~~ m a.s.l., Fig. 1) with sensors to measure SD, air temperature, humidity, air pressure and shortwave radiation (the latter ~~only~~ added in October 2017). The CRS (SnowFox ~~TM~~ ~~TM~~ provided by Hydroinnova [LLC, Albuquerque, NM, USA](#)) is also connected to the station. We ~~have~~ conducted 11 field campaigns over two winter seasons to measure SD and SWE manually. Additionally, we use

Table 1. Sensors ~~used in this study~~ installed at Plaine Morte.

Name	Distributor	Parameter
CNR4	Kipp & Zonen	shortwave radiation
CS215	Campbell Scientific	air temperature, relative humidity
UMB Ventus	Lufft	air pressure, wind speed, wind direction
SnowFox TM (CRS)	Hydroinnova	snow water equivalent (fast neutrons)
SR50A	Campbell scientific	snow depth

observational and gridded meteorological data provided by the Federal Office of Meteorology and Climatology (MeteoSwiss) for comparison and for best-possible data completion. ~~All data are described below in detail,~~ as described below.

2.1 Automatic weather stations

We ~~have~~ installed a five meter high-tall mast on the bare ice of Plaine Morte on which we mounted all sensors (see Table 1) at
5 4.8 m height above the glacier surface. These sensors measured continuously at an hourly interval during two winter seasons
(~~20.10.2016-29.07.2018~~ 20 October 2016 to 29 July 2018). The CRS lies on the bare ice, i.e. below the snowpack, at approxi-
mately 8 m horizontal distance from the mast to avoid-any-limit impacts caused by potential maintenance work.
Precipitation data for comparison to snow accumulation are taken from (i) the federal network of weather stations in Switzer-
land (SwissMetNet, Table 2). ~~The stations are selected according to data quality and the geographic location relative to Plaine~~
10 ~~Morte. Next to the SwissMetNet stations, we also considered stations equipped with a pluviometer of which we selected those~~
~~stations located close to Plaine Morte and with high data quality, and (ii) a gridded precipitation product (RhiresD). We did not~~
~~include precipitation data~~ from the high-elevation weather station network in the Swiss Alps (IMIS, intercantonal measurement
and information system, SLF Data, 2015). ~~However, precipitation observations of selected stations had long as the ones with~~
~~a pluviometer have considerable~~ data gaps during ~~winter and could therefore not be used~~ the winter season.
15 ~~For a further comparison, we also used gridded precipitation from the RhiresD product (MeteoSwiss, 2013). This product~~
~~The gridded precipitation product, RhiresD,~~ uses rain-gauge measurements ~~which are spatially analysed and from around 400~~
automatic as well as manual observations. These observations (not available in real time) are quality-checked prior to their
processing. The observations are spatially analysed, pre-processed and ~~then~~ interpolated to a 1×1 km grid at daily resolution
covering the Swiss territory (MeteoSwiss, 2013). ~~From this dataset we extract time series of the~~ The main sources of uncertainty
20 arise from the interpolation, the rain-gauge measurements, the grid spacing and its effective resolution, and the temporal
variation of the number of stations. For further information, the reader is referred to the technical document provided by
MeteoSwiss (MeteoSwiss, 2013). We extracted daily precipitation estimates of the three grid points closest to the position of
the CRS ~~-(Table 2 and Fig. 1c).~~

Table 2. Table with three meteorological stations with precipitation measurements and three grid cells of the gridded precipitation [product](#). For the gridded precipitation, the coordinate [in EPSG 21781](#) represents the centers of the corresponding pixel ([see Fig. 1](#)).

Station name	Coordinates (WGS 84) [EPSG 21781]	Elevation [m a.s.l.]	Source
Adelboden	609350/149001 46°30'N, 7°34'E	1322	SwissMetNet
Montana	601709/127488 46°18'N, 7°28'E	1427	SwissMetNet
Tsanfleuron	589461/129932 46°19'N, 7°18'E	2052	SwissMetNet
grid cell 1 (H km ¹ km ²)	605500/136500 46°22'N, 7°30'E [605500E, 136500N]	2299	RhiresD
grid cell 2 (H km ¹ km ²)	604500/136500 46°22'N, 7°29'E [604500E, 136500N]	2579	RhiresD
grid cell 3 (H km ¹ km ²)	604500/137500 46°23'N, 7°29'E [604500E, 137500N]	2579	RhiresD

2.2 Field data

Over the two winter seasons 2016/17 and 2017/18, we conducted 11 field campaigns to obtain ~~data for comparison~~ [comparative data](#). During two of ~~these campaigns (20.10.2016 and 05.12.2017)~~, [the campaigns \(20 October 2016 and 5 December 2017\)](#) we installed the CRS ~~-.Because of the disturbed snowpack~~ [which disturbed the snowpack](#). Hence, the measurements of these 5 two campaigns are ~~only used~~ [used only](#) to account for the already ~~existing SWE~~ [fallen snow](#) on the glacier.

During the field campaigns ~~,~~ we measured SWE ~~by means of~~ [using](#) snow pits and snow tube sampling (e.g. Cogley et al., 2011; Kinar and Pomeroy, 2015) and SD ~~with snow probes~~ [by snow probing](#). The snow pits were dug ~~in the vicinity~~ [within approximately 15 meters](#) of the station, but each time at a different location to avoid sampling ~~of~~ a disturbed snowpack.

3 Methods

10 3.1 Filling measurement gaps

~~The measurement period considered in this~~ [This](#) study covers two ~~continuous but highly distinctive~~ [sequential but distinct](#) winter seasons (~~20.10.2016-29.07.2018~~ [20 October 2016 to 29 July 2018](#)). During summer 2017, the ~~weather station AWS~~ on Plaine Morte ~~only measured wind,~~ [measured only wind speed, wind direction,](#) temperature and relative humidity.

In winter 2017/18, unusually high amounts of snow buried most of the mast causing several interruptions of measurements. 15 The time spans of the data gaps differ for ~~the certain~~ sensors because of their measurement characteristics. The SD ~~sensors,~~ [for instance sensor, for example,](#) requires a minimal distance of 0.5 m to the target surface (Campbell Scientific, 2016) and ~~this~~ has the longest data gap. Another issue was the power consumption of the station ~~since when~~ the solar panels ~~were buried~~

~~became buried by snow~~, too. To conserve ~~energy, we turned off power, we deactivated~~ the heated wind sensor (highest energy consumption), which measures wind speed, wind direction, and air pressure. Furthermore, we ~~did not consider disregarded~~ wind speed, temperature and relative humidity from ~~10.03.2018 to 17.04.2018~~ 10 March 2018 to 17 April 2018 because of the proximity of the sensors to the snow surface.

5 ~~Once deployed, the CRS measured reliably~~ The CRS, in contrast, measured continuously over the two winter seasons with ~~one exception~~. ~~During the exception of~~ a short period end of April 2018, ~~the CRS measured irregularly because of a problem with the connector. However~~ 2018. After fixing a faulty connection, the CRS ~~then~~ continued measuring without ~~our interference~~. ~~In summer 2018, we changed the connector and measurements have been without gaps since~~. need for further maintenance.

To fill the data gaps ~~, we correlated the measurements at Plaine Morte with all IMIS stations, we correlated our measurements~~ of the Plaine Morte site with data from the IMIS network and a selection of stations from ~~the~~ SwissMetNet. For ~~the~~ parameters SD, air pressure and wind speed, we chose the station with the highest correlation (Table 3). As SD is an accumulated time series, we correlated the daily change in SD. We did not fill the gap of wind direction because all correlations were below 0.45 at hourly as well as daily ~~scale. Because SD is an accumulated time series, we also correlated the daily change in SD. resolution~~. The mean bias in Table 3 is used to adapt adjust the reference data to the Plaine Morte station. The standard deviation of the
15 mean bias represents the absolute uncertainty of the parameters during the interpolated time period.

3.2 Calculating SWE ~~and the bulk snow density from neutron counts~~

The CRS records the total number of cosmic ray neutrons integrated over a ~~one-hour period~~ set time period, in this case one hour. The neutron ~~intensity, measured count rate expressed~~ in counts per hour (cph) ~~, is then used to infer SWE~~.

~~In a first step, we pre-process obtained neutron counts~~ We process the raw neutron count rate as follows: To eliminate spurious changes in the count rate, neutron counts are excluded if the hourly count differs more than 20% from an 6-hour moving average. ~~The neutron counts are then corrected by~~ As presented in previous literature (e.g. Zreda et al., 2012; Hawdon et al., 2014; Sigouin and ~~, we correct the neutron count rate ($N_{\text{raw},i}$) for time step i for variations in solar activity ($F_{s,i}$) and more importantly by air pressure~~ for changes in situ air pressure ($F_{p,i}$) with

$$\underline{N_i = N_{\text{raw},i} \cdot F_{s,i} \cdot F_{p,i}} \quad (1)$$

25 Variations in solar activity are quantified with the aid of a reference station, which is not buried in the snow (~~Sigouin and Si, 2016; Howat et al., 2016~~). As a reference station ~~, we use the~~ nearby neutron monitor at Jungfraujoch (JUNG, www.nmdb.eu, see Fig. 1) which is located only 40 km from our site. The correction factor F_s is determined as

$$\underline{F_{s,i} = \beta \cdot \left(\frac{F_{\text{inc},i}}{F_{\text{inc},0}} - 1 \right) + 1} \quad (2)$$

30 where variable $F_{\text{inc},i}$ represents the incoming neutron flux at Jungfraujoch (JUNG) at time interval i and $F_{\text{inc},0}$ represents the incoming neutron flux at an arbitrary reference time period. The adjustment factor β depends on the difference in geomagnetic latitude and site elevation between the glacier site and the reference site (Desilets et al., 2006; Hawdon et al., 2014; Andreasen et al., 2017)

Table 3. Time periods of data gaps with reference periods for correlation and correlation coefficients. The mean bias shows the average difference (and its standard deviation) between the reference stations and AWS at Plaine Morte. All stations are shown in Fig. 1

Parameter	Data gap	Reference station Coordinates-Name, Network Coordinates	Correl
snow depth	20.01.2018–04.05.2018 <u>20 Jan 2018 to 4 May 2018</u>	Gandegg/ Laucherenalp (SLFGA2, IMIS) 7°46'E, 46°26'N, 2717 masl <u>SLFGA2, IMIS</u> <u>46°26'N, 7°46'E, 2717 m a.s.l.</u>	04.11.2016–13.07.2017 27.10.2017–19.01.2018 04.05.2018–26.07.2018
air pressure	22.01.2018–10.03.2018 <u>22 Jan 2018 to 10 Mar 2018</u>	Les Diablerets (DIA, SwissMetNet) 7°12'E, DIA, SwissMetNet 46°20'N, <u>7°12'E, 2964 masl</u> <u>m a.s.l.</u>	01.11.2016–22.01.2017 <u>10 Mar 2018</u> 10.03.2018
wind speed	22.01.2018–17.04.2018 <u>22 Jan 2018 to 17 Apr 2018</u>	Guttannen/ Homad (SLFGU2, IMIS) 8°SLFGU2, IMIS <u>46°41'N, 8°17'E, 2110 m a.s.l.</u>	01.01.2018–22.01.2018 17 °E, 46°41'N, 2110 m
temperature	10.03.2018–17.04.2018 <u>10 Mar 2018 to 17 Apr 2018</u>	Les Diablerets (SLFDIA, IMIS) 7SLFDIA, IMIS 46°19'N, <u>7°15'E, 2575 masl</u> <u>m a.s.l.</u>	01.01.2018–10.03.2018 <u>17 Apr 2018</u> 17.04.2018
relative humidity	10.03.2018–17.04.2018 <u>10 Mar 2018 to 17 Apr 2018</u>	Les Diablerets (SLFDIA, IMIS) 7°15'E, SLFDIA, IMIS 46°19'N, <u>7°15'E, 2575 masl</u> <u>m a.s.l.</u>	01.01.2018–10.03.2018 <u>17 Apr 2018</u> 17.04.2018

The manufacturer has provided a value of 0.95 for our site. The adjustment is negligibly small because our study site geographically close to the neutron monitor at Jungfrauoch. Air pressure is directly measured in-situ. More detailed information on the pre-processing of the raw neutron counts is provided in the appendix.

After these corrections, the hourly neutron counts are smoothed using a 6-hour moving average. We calculate SWE from the relation Air pressure is directly measured at the study site. The correction factor $F_{p,i}$ is obtained by

$$F_{p,i} = \exp\left(\frac{p_i - p_0}{L}\right) \quad (3)$$

The mass attenuation length L is assumed to be 132 hPa for our study site and depends on latitude and atmospheric depth (Desilets et al., 2006). The observed hourly pressure values are represented by p_i while p_0 stands for a reference pressure.

Table 4. The constant parameters of Eq. 6. The fitted parameters a_1 , a_2 and a_3 are without unit.

Parameters	Fit
Λ_{\max}	114.4 cm
Λ_{\min}	14.1 cm
a_1	0.313
a_2	0.082
a_3	1.117

For the reference period, we chose a 24-hour time frame between 12 June 2017 at 10 UTC and 13 June 2017 at 10 UTC. The reference variables (N_0 , $F_{\text{inc},0}$, p_0) correspond to the median value during the reference period (Table 5).

To calculate SWE, we use the relative neutron count ($N_{\text{rel},i}$, Eq. 4), i.e. the neutron count (N_i) divided by a reference count (N_0).

$$N_{\text{rel},i} = \frac{N_i}{N_0} \quad (4)$$

The relative neutron count is then used to derive SWE with the non-linear equation

$$SWE_i = -\frac{1}{\Lambda} \cdot \ln \frac{N_i}{N_0}$$

$$SWE_i = -\frac{1}{\Lambda} \cdot \ln N_{\text{rel},i} \quad (5)$$

where N_0 is the mean count rate at snow free conditions, N_i is the hourly count rate, and the variable Λ is the effective attenuation length given by

$$\Lambda_i = \frac{1}{\Lambda_{\max}} \frac{1}{\Lambda_{\max}} + \left(\frac{1}{\Lambda_{\min}} \frac{1}{\Lambda_{\min}} - \frac{1}{\Lambda_{\max}} \frac{1}{\Lambda_{\max}} \right) \cdot \left(1 + \exp \left(-\frac{\frac{N_i}{N_0} - a_1}{a_2} \frac{N_{\text{rel},i} - a_1}{a_2} \right) \right)^{-a_3} \quad (6)$$

The empirical parameters that were provided by the manufacturer are Λ_{\min} (14.1 cm) and Λ_{\max} (114.4 cm), Λ_{\min} , Λ_{\max} , a_1 (0.3), a_2 (0.1) and a_3 (1.1) Table 4) were provided by the manufacturer for use on glaciers and were also used by Howat et al. (2018)

Note that the parameters Λ_{\min} and Λ_{\max} are respectively the asymptotic values of the effective attenuation lengths for low and high SWE values, and that the parameters a_1 , a_2 and a_3 define the curvature of a sigmoidal function. The reference count rate

In this study, we report daily estimates of SWE. The direct observations, however, are based on hourly values. Therefore, we integrated the mean daily neutron counts of $N_{\text{raw},i}$. N_0 is determined over the median count rate in July 2017 (4146 cph).

Fig. 2a shows the theoretical exponential relation between hourly neutron counts and SWE given by Eq. 5. $F_{\text{inc},i}$, $F_{\text{inc},0}$ over 24 hours and took the mean daily pressure for p_i to calculate SWE.

From the hourly SWE values, we calculate the daily means (SWE_{crs}).

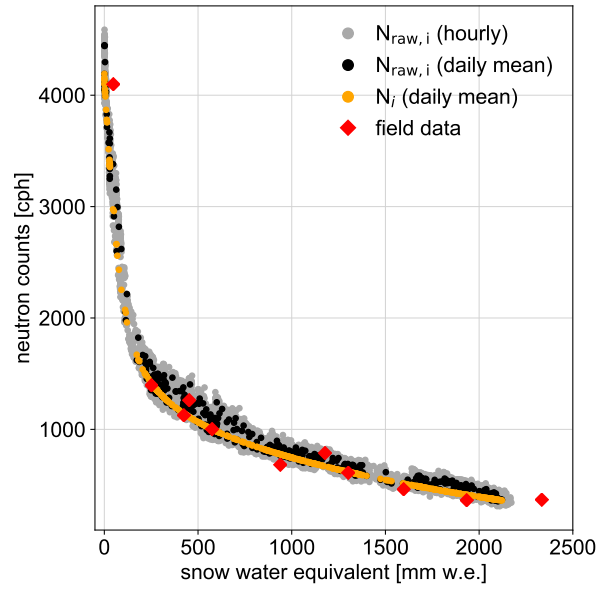


Figure 2. (a) Hourly Relation between SWE and the neutron count rate. Grey dots represent the uncorrected hourly neutron counts (corrected and smoothed) with calculated SWE amounts (grey-black dots) the uncorrected daily means. Black-The orange dots show represent the average-corrected daily neutron counts with average-daily-SWE amounts means. Red crosses-dots show field-measurements of SWE from the field data and their-the corresponding daily-neutron counts. The error-bars refer to the uncertainties. The green-line shows the theoretical SWE amounts with the applied N_0 . Panel (b) shows the daily uncertainty of SWE ($\sigma_{SWE_{CRS}}$) for all observed daily SWE amounts. The green-line represents the theoretical-increase-in-uncertainty-with-SWE field work days.

3.3 Calculating snow density and daily changes in SWE, SD and snow density

The bulk snow density ($\rho_{crs, sr}$, in kg m^{-3}) is then derived from daily SWE (SWE_{crs} , in kg m^{-2}) (SWE_{crs} , in mm w.e. or kg m^{-2}) and daily SD measurements (SD_{sr} , in cm) according to

$$\rho_{crs, sr} = \frac{SWE_{crs}}{SD_{sr}} \cdot c \quad (7)$$

5 with c equal to 100 cm m^{-1} to assure unit consistency.

The temporal resolution of one day allows the determination of daily changes in SD, SWE and the bulk snow density. These daily changes are calculated as the difference between two consecutive days. To assure the exclusion of errors, the daily rates have to be larger than the uncertainty estimates (see below). We filtered out days where daily changes were lower than the uncertainty estimates.

10 3.4 Estimating the uncertainty of the CRS

The calculated SWE is determined by the corrected neutron count relative to when the CRS is uncovered by snow ($N_{rel,i}$, Eq. 4). We base our error propagation on all corrections applied to the raw neutron count. We assemble Eq. 1-4 into

$$N_{rel,i} = N_{raw,i} \cdot \left(\beta \cdot \left(\frac{F_{inc,i}}{F_{inc,0}} - 1 \right) + 1 \right) \cdot \exp\left(\frac{p_i - p_0}{L}\right) \cdot \frac{1}{N_0} \quad (8)$$

The raw neutron count ($N_{raw,i}$), the incoming neutron flux ($F_{inc,i}$) and air pressure (p_i) change with time, but remain independent from each other. Following the rules of error propagation of a non-linear equation, we approximate the uncertainty in $N_{rel,i}$ as

$$\begin{aligned} \sigma_{N_{rel,i}}^2 \approx & \left(\frac{\partial N_{rel,i}}{\partial N_{raw,i}} \right)^2 \cdot \sigma_{N_{raw,i}}^2 + \left(\frac{\partial N_{rel,i}}{\partial N_0} \right)^2 \cdot \sigma_{N_0}^2 \\ & + \left(\frac{\partial N_{rel,i}}{\partial F_{inc,i}} \right)^2 \cdot \sigma_{F_{inc,i}}^2 + \left(\frac{\partial N_{rel,i}}{\partial F_{inc,0}} \right)^2 \cdot \sigma_{F_{inc,0}}^2 + \left(\frac{\partial N_{rel,i}}{\partial \beta} \right)^2 \cdot \sigma_{\beta}^2 \\ & + \left(\frac{\partial N_{rel,i}}{\partial p_i} \right)^2 \cdot \sigma_{p_i}^2 + \left(\frac{\partial N_{rel,i}}{\partial p_0} \right)^2 \cdot \sigma_{p_0}^2 + \left(\frac{\partial N_{rel,i}}{\partial L} \right)^2 \cdot \sigma_L^2 \end{aligned} \quad (9)$$

The uncertainty $\sigma_{N_{rel,i}}^2$ is then propagated through Eq. 5 to estimate the uncertainty $\sigma_{crs,i}$.

$$\sigma_{crs,i} \approx \sqrt{\left(\frac{\partial SWE_i}{\partial N_{rel,i}} \right)^2 \cdot \sigma_{N_{rel,i}}^2} \quad (10)$$

Since the uncertainties are not always known, we assume rather generous estimates for the uncertainties of all correction factors. Table 5 provides an overview of uncertainty estimates for all components.

For all neutron count rates ($N_{raw,i}$, N_0 , $F_{inc,0}$, $F_{inc,i}$), we assume poissonian counting statistics, which gives the uncertainty as the square root of the neutron counts (e.g. Zreda et al., 2012). With the integration over a time period t , the uncertainty is reduced by $t^{-0.5}$ (Schrön et al., 2018). While the relative uncertainty in $N_{raw,i}$ varies between 1.5%-5.3% for hourly observations, it varies between 0.3%-1% for the integrated daily estimates of our study.

The incoming radiation measured at Jungfrauoch has a low statistical uncertainty as its precision is high with around 190 counts per second. However, incoming radiation is corrected by an adjustment factor (β , Eq. 2) which is rather small for our site. Therefore, we assume also a small uncertainty of 0.03 for σ_{β} .

The uncertainty in air pressure (σ_{p_i} , σ_{p_0}) is based on the instrumental precision of 0.1 hPa (Lufft, 2019). For the mass attenuation length L , we use 132 hPa. An applied uncertainty of ± 2 hPa corresponds to the difference of shielding depths from latitudes north and south of Switzerland as shown in Fig.1 of Andreassen et al. (2017).

To render the error propagation more robust, we calculated $\sigma_{crs,i}$ using two different time resolutions. We additionally created a synthetic data set for both time resolutions. For the synthetic data set, we varied the time-dependent variables ($N_{raw,i}$, p_i , $F_{inc,i}$) uniformly within their observed minima and maxima values. At the hourly resolution it encompasses $4.8 \cdot 10^5$ hours and at the daily resolution it encompasses $4.8 \cdot 10^5$ days.

Figure 3a and b show the resulting precision for an hourly and daily resolution, respectively. Figure 3c and d show the relative contribution of every uncertainty term in Eq. 9, i.e. a high relative contribution indicates that the given parameter is an

Table 5. Compilation of all direct observations and constants as well as the associated uncertainties σ at the hourly and daily scale. The units cph and cps stand for counts per hour and second, respectively. Brackets show the minimum and maximum within the time series.

<u>Variables</u>	<u>hourly values</u>	<u>σ (hourly)</u>	<u>σ (daily)</u>
$N_{\text{raw},i}$	[354; 4450] cph	$\sqrt{N_{\text{raw},i}}$ cph	$\sqrt{\frac{N_{\text{raw},i}}{24}}$ cph
N_0	4143 cph	64 cph	13 cph
$F_{\text{inc},i}$	[184; 195] cps	$\sqrt{\frac{F_{\text{inc},i}}{3600}}$ cps	$\sqrt{\frac{F_{\text{inc},i}}{86400}}$ cps
$F_{\text{inc},0}$	191 cps	0.2 cps	0.1 cps
β	0.95	0.03	0.03
p_i	[708; 747] hPa	0.1 hPa	0.1 hPa
p_0	739 hPa	0.1 hPa	0.1 hPa
L	132 hPa	2 hPa	2 hPa

important source for the overall uncertainty of SWE. Figure 3 shows that the main uncertainty can be attributed to the neutron count uncertainty, independently of the time resolution. However, the precision estimate presented here does not include the uncertainty of the correction parameterization (Eq. 2 and Eq. 3) or the conversion equation (Eq. 5) and its parameters (Table 4).

5 3.5 Estimating the uncertainty of automatically derived SWE, SD and snow density

In general, we distinguish between the observed standard deviation of all observed hourly values during one day (s) and the theoretical measurement ~~uncertainty-precision~~ in those daily values (σ). The daily standard ~~deviations-deviation~~ of SWE ($s_{\text{SWE}_{\text{crs}}}$, $s_{\text{SWE}_{\text{crs}}}$) and SD ($s_{\text{SD}_{\text{sr}}}$, $s_{\text{SD}_{\text{sr}}}$) are derived assuming a gaussian distribution. For the standard deviation of the bulk density ($s_{\rho(\text{crs}_{\text{sr}})}$, $s_{\rho(\text{crs}_{\text{sr}})}$), we apply gaussian error propagation to Eq. 7 to yield

$$10 \quad s_{\rho(\text{crs}_{\text{sr}})} = \sqrt{\left(\frac{s_{\text{SWE}_{\text{crs}}}}{\text{SWE}_{\text{crs}}}\right)^2 + \left(\frac{s_{\text{SD}_{\text{sr}}}}{\text{SD}_{\text{sr}}}\right)^2} \sqrt{\left(\frac{s_{\text{SWE}_{\text{crs}}}}{\text{SWE}_{\text{crs}}}\right)^2 + \left(\frac{s_{\text{SD}_{\text{sr}}}}{\text{SD}_{\text{sr}}}\right)^2} \quad (11)$$

The calculation of the measurement uncertainties of SD (σ_{sr}), SWE (σ_{crs}) and the bulk density ($\sigma_{\rho(\text{crs}_{\text{sr}})}$) is described in the following paragraphs. ~~The main source of uncertainty in the SWE estimates (σ_{crs}) is the neutron count uncertainty. This uncertainty is given by-~~

$$\sigma_{N_i} = \sqrt{N_i}$$

15 ~~and is valid for all temporal resolutions (i). Applying the general error propagation formula on Eq. 5, we derive-~~

$$\sigma_{\text{crs}} = \left(\frac{\partial \text{SWE}_{\text{crs}}}{\partial N}\right) \cdot \sigma_N + \sigma_{\text{const}}$$

~~Because the fluctuations of SWE estimates in snow free conditions are ± 0.5 cm around 0 cm of snow, we add an additional constant uncertainty of ± 1 cm (σ_{const}). In this study, the calculation of the theoretical uncertainty of the SWE observations is~~

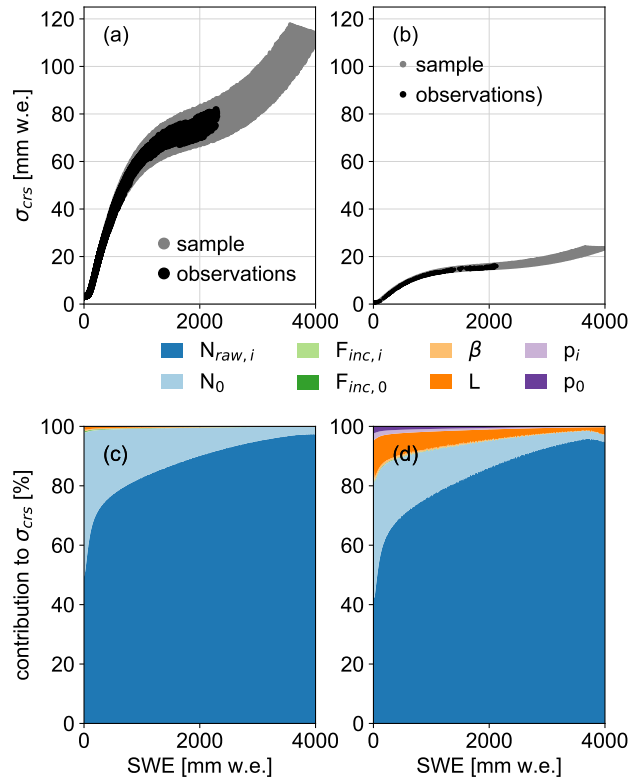


Figure 3. Precision of SWE calculated by means of error propagation. (a) and (b) show the absolute precision with grey dots as a synthetic data set and black dots as the in situ observations. (c) and (d) show the relative contribution of each parameter to the overall precision. (a) and (c) present the results based on hourly observations while (b) and (d) show the results of the daily observations.

done at the daily resolution. Fig. 2a shows the uncertainty of the daily neutron counts and daily SWE values. Fig. 2b shows the theoretical uncertainty and the daily observed uncertainties, which are lower than in theory. The outliers at round 200 cm SWE result from a short measurements gap end of April 2018. During this gap, some hourly values were missing resulting in an overall lower daily neutron count and a consequently higher uncertainty. We also note that the relative error in SWE slowly decreases with higher SWE amounts. For instance, it is 2% at 100 cm, but 1.3% at 200 cm of SWE.

The uncertainty of the daily SD observations varies with the depth of the snowpack. According to the installation manual, the accuracy lies between ± 1 cm and 0.4% of the distance from sensor to ground (Campbell Scientific, 2016). Since the sensor is mounted at 4.754.8 m, the maximum uncertainty equals 1.9 cm under snow free conditions. In addition to the given uncertainty, we add a further systematic measurement uncertainty on SD's less than 30 cm. This uncertainty is because caused by the footprint of the sonic ranging sensor which is large enough to include parts of the mast's foundations. The mast's foundation consists of three wooden beams with a height of 20 cm each. Their function is to They stabilize the mast on the glacier ice, especially during the ice melt season. To keep the wooden beams in place, they are anchored with tubes

drilled into the ice. These tubes also exceed the 20 cm height of the wooden beams and add an additional error. We estimate this additional uncertainty to be 30% with SD below 30 cm, 50% with SD below 25 cm, 80% with SD below 15 cm and 100% with SD below 10 cm. Moreover, the SD measurements from ~~20.01.2018 to 04.05.2018~~ 20 January 2018 to 4 May 2018 which have been taken from another station at high-elevation carry an additional uncertainty of 6 cm (see Table 3).

- 5 Using the uncertainties of SD and SWE, we derive the uncertainty of the daily bulk density (σ_{ρ}) as

$$\sigma_{\rho(\text{crs, sr})} = \sqrt{\left(\frac{\sigma_{\text{crs}}}{\text{SWE}_{\text{crs}}}\right)^2 + \left(\frac{\sigma_{\text{sr}}}{\text{SD}_{\text{sr}}}\right)^2} \sqrt{\left(\frac{\sigma_{\text{crs}}}{\text{SWE}_{\text{crs}}}\right)^2 + \left(\frac{\sigma_{\text{sr}}}{\text{SD}_{\text{sr}}}\right)^2} \quad (12)$$

3.6 Estimating the uncertainty of field data

Field measurements carry uncertainties ~~-, which may have different from a variety of~~ sources (sampling tube, weight scale, sampling technique, etc.). ~~Only few~~ Few studies discuss the accuracy of SWE observations comprehensively (e.g. Stuefer et al., 2013). Commonly, a relative uncertainty of $\pm 10\%$ is applied (e.g. Schattan et al., 2017). Thibert et al. (2008), for example, focus on uncertainties for glacier mass balance calculations based on the glaciological method. These random and systematic errors, however, assume underlying firn with unknown water content and are not intended for snow accumulation. For our study, we have chosen to calculate an uncertainty based on the gaussian error propagation (see Papula, 2010). Next to the human-induced errors, which cannot be quantified in the scope of this study, we identify two major sources of sampling errors. These are related to the weighed mass and the snow volume within the tube.

We sample an entire column of the snowpack ~~-,~~ from the surface to the snow-glacier interface. These samples are taken either within a snow pit ~~-,~~ or by extracting a snow core. In both approaches ~~-,~~ we use a sampling tube. In deeper snowpacks ~~-,~~ the whole column cannot be sampled in one measurement step. Thus ~~-,~~ we take several samples with a certain length (l_s) from snow to glacier surface. For each of these samples ~~-,~~ the density (ρ_s) is calculated by applying Eq. 13). The variable m_s represents the mass of the snow weighed ~~in-situ in situ~~ with a scale ~~-,~~ while r_{tube} represents the radius of the sampling tube.

$$\rho_s = \frac{m_s}{\pi \cdot r_{\text{tube}}^2 \cdot l_s} \quad (13)$$

The sources of the sample uncertainty in density (σ_{ρ_s}) arise from the uncertainties in snow-mass weighing (Σm_s), the uncertainties of the sampled volume given by the radius (Σr_{tube}) and the uncertainties of the sampled length (Σl_s) in the snowpack. The uncertainty of the mass is thus composed of two individual sources; the scale for weighing the sample (Σm_{scale}), and the extracted snow volume (Σm_{mass}). These two uncertainties are added to Σm_s following Gaussian error propagation. Because the surface area of the extracted snow core does not always match the tube's surface area, we define an uncertainty range for the radius. The relative uncertainty of each sample (σ_{ρ_s}) is then derived from

$$\sigma_{\rho_s} = \frac{\Sigma \rho_s}{\rho_s} = \sqrt{\left(\frac{\Sigma m_s}{m_s}\right)^2 + \left(2 \cdot \frac{\Sigma r_{\text{tube}}}{r_{\text{tube}}}\right)^2 + \left(\frac{\Sigma l_s}{l_s}\right)^2} \quad (14)$$

Given the density for each sample at different depths within the snowpack, we calculate the bulk density ($\rho_{\text{field}} \rho_{\text{field}}$). To this end, we need to divide the snowpack into layers of variable lengths. Because of this variation, we determine a multiplicative weight $p_{\text{t}} p_{\text{t}}$ for each layer as

$$p_{\text{t}} = \frac{l_{\text{t}}}{SD_{\text{field}}} \frac{l_{\text{t}}}{SD_{\text{field}}} \quad (15)$$

- 5 This weight corresponds to the relative contribution of l_{t} to the total depth of the snowpack ($SD_{\text{field}} SD_{\text{field}}$) which is measured independently.

The samples may overlap depending on the tube and the extraction method used. If there is no overlap, the length of the sample $l_{\text{s}} l_{\text{s}}$ is equal to the length-thickness of the layer $l_{\text{t}} l_{\text{t}}$, and the number of samples is equal to the number of layers ($n_{\text{t}} n_{\text{t}}$). Simultaneously, the sample density ($\rho_{\text{s}} \pm \Sigma \rho_{\text{s}} \rho_{\text{s}} \pm \Sigma \rho_{\text{s}}$) corresponds to the layer density ($\rho_{\text{t}} \pm \Sigma \rho_{\text{t}} \rho_{\text{t}} \pm \Sigma \rho_{\text{t}}$). If the samples overlap, $p_{\text{t}} p_{\text{t}}$ corresponds to the mean density and propagated uncertainty of the overlapping samples. In that case, the number of layers is greater than the number of samples. With

$$\rho_{\text{field field}} = \frac{1}{n_{\text{t}}} \frac{1}{n_{\text{t}}} \cdot \sum_{i=1}^{n_{\text{t}} n_{\text{t}}} p_{1,i} \cdot \rho_{1,i} \quad (16)$$

and

$$\sigma_{\rho_{\text{field field}}} = \frac{\Sigma \rho_{\text{field}}}{\rho_{\text{field}}} \frac{\Sigma \rho_{\text{field}}}{\rho_{\text{field}}} = \frac{\sqrt{\sum_{i=1}^{n_{\text{t}} n_{\text{t}}} p_{1,i} \cdot (\Sigma \rho_{1,i})^2} \sqrt{\sum_{i=1}^{n_{\text{t}} n_{\text{t}}} p_{1,i} \cdot (\Sigma \rho_{1,i})^2}}{\rho_{\text{field field}}} \quad (17)$$

- 15 we obtain the bulk density ($\rho_{\text{field}} \rho_{\text{field}}$) and its relative uncertainty ($\sigma_{\rho_{\text{field}}} \sigma_{\rho_{\text{field}}}$).

Knowing the bulk density and the depth of the snowpack ($SD_{\text{field}} SD_{\text{field}}$), we calculate the total amount of SWE ($SW E_{\text{field}}$) with total SWE ($SW E_{\text{field}}$) with

$$SW E_{\text{field field}} = \rho_{\text{field field}} \cdot SD_{\text{field field}} \quad (18)$$

With error propagation by Gauss, gaussian error propagation we derive the relative uncertainty of SWE as

$$20 \sigma_{\text{SWE}_{\text{field field}}} = \frac{\Sigma SW E_{\text{field}}}{SW E_{\text{field}}} \frac{\Sigma SW E_{\text{field}}}{SW E_{\text{field}}} = \sqrt{\left(\frac{\Sigma \rho_{\text{field}}}{\rho_{\text{field}}}\right)^2 + \left(\frac{\Sigma SD_{\text{field}}}{SD_{\text{field}}}\right)^2} \sqrt{\left(\frac{\Sigma \rho_{\text{field}}}{\rho_{\text{field}}}\right)^2 + \left(\frac{\Sigma SD_{\text{field}}}{SD_{\text{field}}}\right)^2} \quad (19)$$

The absolute uncertainty of SD_{field} ($\Sigma SD_{\text{field}} \Sigma SD_{\text{field}}$) is estimated independently of the sample measurements. The absolute uncertainty of the bulk density ($\Sigma \rho_{\text{field}} \Sigma \rho_{\text{field}}$) is given in Eq. 17.

For each field campaign we define the discussed uncertainty depending uncertainty based on the sampling tube, the scale, and whether we sampled within a snow pit or extracted a snow core. Thereby, we use four different We used tubes with a radius radii of 4.00 ± 0.10 cm, 4.15 ± 0.15 cm, 4.50 ± 0.10 cm and 4.75 ± 0.10 cm and a length lengths of 117.0 cm, 107.0 cm, 55.7 cm and 56.0 cm, respectively. Additionally, we have three scales with a maximum weighing capacity of 2 ± 0.02 kg, 5 ± 0.05 kg and 12 ± 0.10 kg. The uncertainty in the weighed mass ranges from 0.05 kg to 0.15 kg depending on the snow depth and the tube

length. Sampling lengths are attributed ~~with an uncertainty between an uncertainty from~~ 0.5 cm ~~and to~~ 1.0 cm. During a ~~field campaign, campaign~~ we usually sample more than one ~~snow~~ column. In those cases we take an average of all snow ~~parameters, and we average all σ to account for variables and average all uncertainties to yield~~ the mean uncertainties. We quantify the variability within several snow columns with their standard deviation (s) which is smaller than the mean uncertainty. An
5 extensive table on all assumed uncertainties, the number of samples per snow pit is provided in the supplement.

3.7 Pre-processing ~~and~~ precipitation ~~data~~scaling

~~Precipitation data from nearby~~ ~~In the final part of this study we estimated the optimal scaling factor for precipitation amounts from three~~ stations at lower elevations ~~are compared to snow accumulation observed by the CRS. The precipitation data have an hourly resolution measured and for three grid cells of the gridded precipitation (Table 2).~~

10 ~~Because snow accumulation is cumulative and precipitation is instantaneous we first sum the hourly precipitation amounts to daily amounts over the whole winter seasons from HH:01 to (HH+1):00. To compare it, we sum the hourly values to daily precipitation amounts. The time series of the precipitation sums begins~~ ~~Second, we adjust the cumulative precipitation to the amounts of snow accumulation at the beginning of the season. In the first winter season (2016/17), precipitation records begin at the same~~ ~~day as the time as~~ snow accumulation observations. ~~That implies adding a constant value~~ ~~In the second winter~~
15 ~~season (2017/18), observations by the CRS began when the snowpack was already developed. To start the observations of snow accumulation and cumulative precipitation at the same level, we add a constant offset to the cumulative precipitation series in the second winter because the snowpack was already advanced when observations began. This offset corresponds to the first SWE amount measured by the CRS in the respective winter.~~ The end of the ~~precipitation~~ time series is set at the end of May for ~~each year~~ ~~both years~~. At this point in time, the peak of SWE had already passed in both winters.

20 ~~To find a suitable scaling factor, all daily precipitation sums are multiplied by the same scaling factor and compared to the snow accumulation. In the second winter season, we also add a constant factor so that snow accumulation and precipitation begin with the same amounts. The comparison is analyzed by the~~ ~~In a first analysis we apply scaling factors between 0.1 and 8.1 at an 0.1 interval to all daily instantaneous precipitation observations. We then accumulate the scaled daily precipitation over the winter season. Compared to 392 days of CRS observations, we calculate the daily absolute error and derive the seasonal~~
25 ~~mean absolute error (MAE) and its standard deviation over the whole time series at the daily resolution. For each station, we have 392 days available for comparison. We then chose the scaling factors resulting in the lowest MAE for all AWS and grid cells.~~

In a ~~more elaborate approach, hourly temperature data from the station at Plaine Morte is included. Therefore, we categorize days with only liquid, only solid, and a mixture between liquid and solid precipitation. For the distinction, we introduce~~
30 ~~temperature thresholds based on previous studies~~ ~~second analysis we find the optimal scaling factor for each precipitation phase, i.e. solid, liquid and mixed-phase. The precipitation phases are defined through air temperature observations at the glacier site. This parameterization of precipitation phases is based on values from literature.~~ The study by Sims and Liu (2015), for instance, show that 90% of precipitation events were solid precipitation for near-surface temperatures below 0°C for land surface observations. For temperatures above 3°, more than 85% of all precipitation events were liquid. ~~Therefore~~ ~~Hence~~, we

consider all precipitation as liquid if temperatures are above 3°C during at least six hours. If temperatures ~~range-remain~~ between 0°C and 3°C during at least six hours, we classify it as mixed-phase precipitation. ~~Thereby, all days with such a classification are used to determine the optimal scaling factor. If the two previous criteria do not apply or the daily maximum temperature does not exceed 0°C, it is solid precipitation. For these classified days, we evaluate the optimal scaling factor applying the~~
5 ~~same procedure as described~~ Solid precipitation only occurs with subzero temperatures. For each of these phases, we apply the procedure described in the analysis above.

4 Results

4.1 Measured ~~snow depth~~SD, SWE and snow density

With the CRS installed on Plaine Morte, SWE was measured during two subsequent winter seasons (2016/17 and 2017/18).
10 These two winters were markedly different, ~~with~~. The first winter received typical snowfall while the second winter ~~experiencing~~ experienced particularly heavy snowfall. During winter 2016/17, a maximum SD of 324 cm was reached on ~~02.05.2017~~ 2 May 2017 and a maximum SWE (~~137 cm~~ 1379 mm w.e.) on ~~18.05.2017~~ 18 May 2017. With these observations, the first winter season lies in the range of average mean specific winter mass balances between 2009 to ~~2017~~ 2019 (GLAMOS, 1881-2018). During the ~~following winter~~ second winter (2017/18), a maximum of ~~520~~ 527 cm of SD (~~01.04.2018~~ 1 April 2018) and a
15 maximum SWE of ~~212 cm~~ 2122 mm w.e. (~~24.05.2018~~ 24 May 2018) were observed, which corresponds to ~~about~~ approximately 1.5 times of ~~SWE than in the~~ SWE amount of the previous year.

~~Fig-Figure~~ Figure 4a and ~~e-show~~ b show the snow accumulation and ablation over the two winter seasons. In both winters, the first snowfall ~~around-occurred~~ mid-October ~~led to SDs when SDs reached~~ of about 20 cm. By mid-November, SD exceeded one meter with ~~approximately 30 cm~~ a SWE amount of approximately 300 mm w.e. in both winters. ~~While there was no further~~
20 ~~snow accumulation in~~ In winter 2016/17, ~~the SD remained almost constant~~ until the beginning of January, ~~the SD tripled itself by 2017~~. In the following winter, SD significantly increased from November 2017 to January 2018. By that time, it had already surpassed the maximum in SD of the previous winter.

From January 2017 to ~~Mai~~ May 2017, SD increased almost ~~regularly~~ continuously with a period of accumulation followed by a period of densification. The time lag between the maximum of SD and the maximum of SWE is 16 days. During this
25 time span, SWE remained almost constant and only increased little. By the beginning of July 2017, the snow had completely melted. In winter 2017/18, SWE increased more continuously between end of January and beginning of June. In this winter, the maxima in SD and SWE are almost two months apart. Already in April 2018, SD started decreasing while SWE remained constant. During that time, only few events led to small increases in SD. From end of Mai 2018 onwards, SWE decreased rapidly. By the end of July, the snow had disappeared.

30 ~~With the daily observations of SWE and SD, we calculate the daily bulk snow density. Fig. 4b and d show its evolution over time.~~ In the beginning of winter 2016/17, ~~for instance~~, snow density increases after a short decrease ~~-(Fig. 4c)~~. This short increase corresponds to the snowfall observed in Fig. 4a and b. In general, densification slowly progresses with short intervals of decreasing densities caused by ~~snow fall~~ snowfall. Between the maximum SD and the maximum SWE, density increases

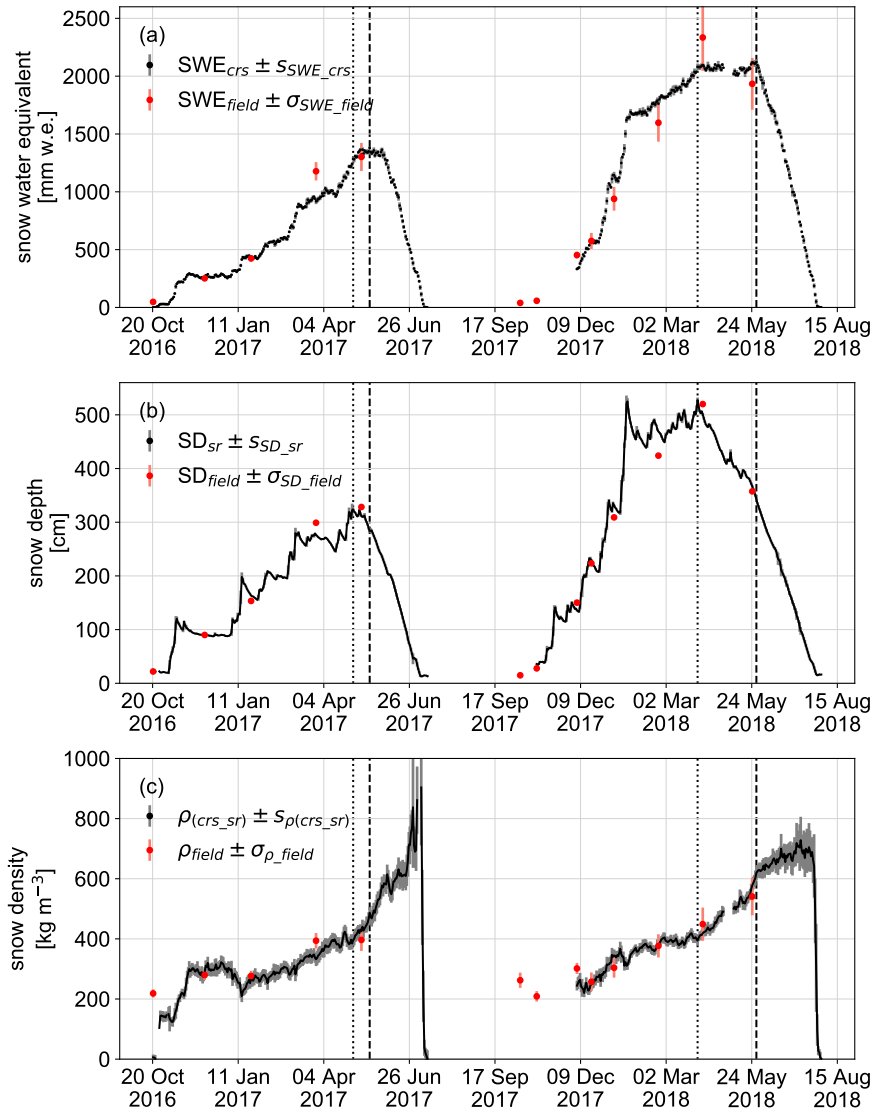


Figure 4. Blue squares show the evolution Continuous observations of snow depth (SD), green dots the evolution of SWE during winter 2016/17 (a) and winter 2017/18 (c). The shading corresponds to the theoretical uncertainty while bars represent the daily standard deviation. Red squares and dots (a,c) represent manual measurements of SD and SWE, respectively. Salmon bars show the uncertainty of the field measurements. (b) SD and (d) show the temporal evolution the mean snow density with its uncertainty (orange shading) their daily standard deviation. Red diamonds The red dots show the manual field measurements with their uncertainty uncertainties (salmon bars). The dotted (dashed) line shows the day of the seasonal maxima in SD (SWE).

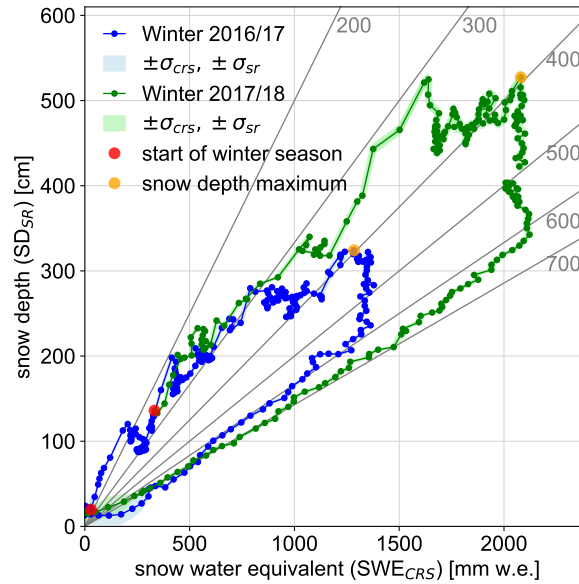


Figure 5. Daily mean SWE and daily mean SD. Grey lines show the densities in kg m^{-3} . The beginning of each winter season is marked by the red dot, yellow dots indicate the maximum of SD.

almost linearly in both winters. After reaching the maxima of SWE, snow densities are above 500 kg m^{-3} . Shortly before the snowpack disappears completely, densities decrease ~~but carry larger uncertainties rapidly~~. The comparatively high standard deviations of the snow density (Fig. 4c) are a consequence of the daily variability in SD. SD may decrease significantly during a day when densification rates are strong while SWE remains constant.

- 5 Fig.Figure 5 shows daily SWE in relation to daily SD over the winter season. During the accumulation period, daily densities ~~lie vary~~ between 200 kg m^{-3} and 400 kg m^{-3} . ~~Often, an An~~ increase in SD is ~~often~~ followed by a period ~~where SWE remains constant and SD decreases. This marks periods of constant SWE and decreasing SD which is characteristic~~ of snow densification. ~~In general, both winters~~ Both winters tend to follow a similar pattern in the evolution of density. At the maximum of SD, the daily density is 390 kg m^{-3} for winter ~~162016/17 (02.05.2017) May 2017~~ and 392 kg m^{-3} for winter ~~172017/18 (01.04.2018) April 2018~~.
- 10 ~~After these peaks, the snowpack enters a period of densification, which is identifiable for both winters~~ begins to densify continuously. During this period of densification, SWE remains almost constant while SD decreases by about 1 m (2016/17) and 1.5 m (2017/18). Only then does ~~the~~ SWE begin to decrease simultaneously with SD, following the density lines between 600 kg m^{-3} and 700 kg m^{-3} .

- For the evaluation of the CRS, we ~~obtained field data during 11~~ use field data from nine campaigns over the two winter
- 15 seasons. Fig.Figure 6 shows the autonomous data of SWE (Fig. 6a), SD (Fig. 6b) and snow density (Fig. 6c) compared to the data from the field surveys. On average, the CRS overestimates SWE by $+2\% \pm 12\%$. The ~~sonic ranger agrees SD~~ measurements agree within a standard deviation of $\pm 6\%$, and $\pm 7\%$ when also considering the interpolated data during the

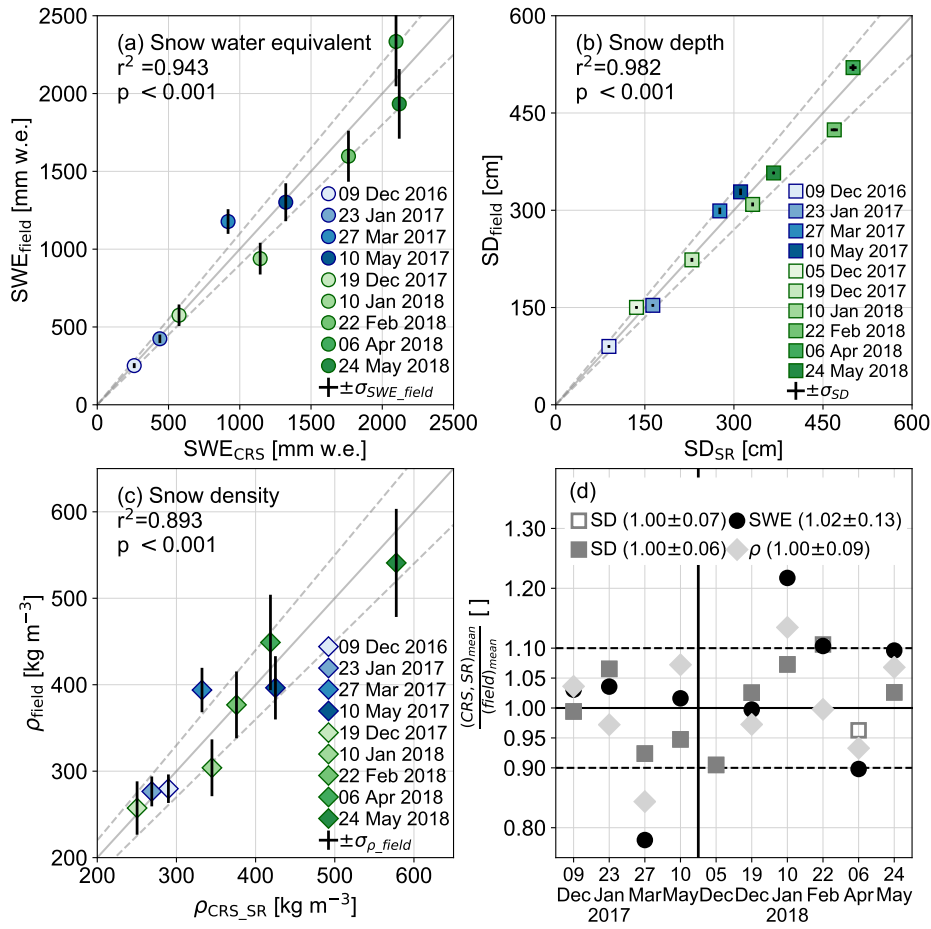


Figure 6. Scatter plots of the field data compared to the automatic-autonomous measurements of SWE-(a) SWE, SD-(b) SD and bulk-snow density-(c) bulk snow density. The dashed grey lines show the range within $\pm 10\%$. The error bars correspond to the uncertainty of the field data only for SWE and snow density. (d) shows the relative-differences-for-each-ratio between field campaign-and-automatic measurements for SD, SWE and snow density (ρ). The unfilled grey squares represent the data interpolated from another station.

measurement gap of SD. The snow density data agree on average with a standard deviation of $8 \pm 9\%$ (Fig. 6d). Furthermore, the uncertainties of the field data are always higher than the estimated uncertainties of the automatic measurements. This is due to the higher precision of the automatic measurements, the undisturbed snowpack, and the exclusion of potential human-induced errors. The correlation coefficients (r^2) of all considered snowpack parameters are higher than 0.90-0.89 (Fig. 6).

5 4.2 Daily variations of SWE-and-SD and SWE

From-With the continuous data of SWE and SD, we can-evaluate the daily variations -of snow properties (Fig. 7 ashows this day-to-day variations of SWE and SD. With this information, we can distinguish days dominated by general processes affecting

Table 6. ~~Definition-Overview~~ of ~~all considered processes, their criteria and~~ the ~~process-dominated-number of days with-when~~ the ~~color criteria are fulfilled. The colors refer to the processes~~ displayed in Fig. 7; ~~the criteria and the number of days~~.

Process	color	snow depth	SWE	days (2016-2018)	days (2016/17)	days (2017/18)
all	-	-	-	484-487 (100%)	260 (100%)	224-227 (100%)
accumulation	lightblue	$> \sigma_{sr}$	> 0 cm	112-231 (22%)	58-56 (22%)	54-2451 (22%)
ablation	red	$< -\sigma_{sr}$	$< -\sigma_{crs}$	73-110 (23%)	28-1148 (18%)	45-2062 (27%)
densification	green	$< -\sigma_{sr}$	≥ 0 cm	210-431 (36%)	101-3980 (31%)	109-4994 (41%)
not classified	white	-	-	89-1896 (20%)	73-2876 (29%)	16-720 (9%)
subgroups						
accumulation (high confidence)	blue	$> \sigma_{sr}$	$> \sigma_{crs}$	61-81	32-47	29-34
densification with accumulation	lightgreen	≤ 0 cm	$> \sigma_{crs}$	28-74	1443	1431

the snowpack such as). We use this to classify days based on whether they were dominated by accumulation, densification and ablation. To this end or ablation. For this purpose, we define a criterium-criteria for SWE and SD considering the uncertainties of the measurements. The uncertainties are especially precision estimates of the observations. The precision is especially important for the SWE measurements important as because we want to distinguish between noise and signal. Table 6 gives an overview of all criteria and the number of days when these are satisfied/fulfilled. A day dominated by accumulation has to have a change in SD greater σ_{sr} , while the change in SWE has to be greater than 0 cm. To ensure more confidence (accumulation with high confidence), the SWE changes have to exceed σ_{crs} (Table 6). The same applies for ablation with the difference that the daily change has to be more negative than the uncertainty values. For densification, we require a significant decrease in SD while SWE remains constant or increases. For the latter case, we extract the days where densification and accumulation happen occur on the same day. Fig-Figure 7b shows that the winter is mainly dominated by accumulation and densification. Some days with ablation occur at the beginning of March 2017. On these days, we note higher wind gusts and subzero temperatures (Fig. 7c and d). Hence, ablation is likely caused by wind-snow drift rather than melt. Ablation through snow-melt sets in as soon as daily air temperatures are above 0 °C.

The mean daily meteorological conditions can be summarized for the categorized days (Fig. 8, Tab-Table 6). Days with accumulation are characterized by high relative humidity (Fig. 8a), significantly lower temperatures (Fig. 8b) and an average decrease in mean density (Fig. 8c). Wind speeds are higher often above 6 m s^{-1} and originate mainly from south over west to north. Days dominated by ablation are characterized by average daily relative humidity (Fig. 8a), significantly higher temperatures (Fig. 8b) and lower wind speeds-wind speeds that are mainly around or below 4 m s^{-1} (Fig. 8d). During the ablation days, we find no significant change in density. Days with densification have lower daily relative humidities are drier than days with ablation. The median values of daily mean temperatures and daily mean wind speeds are similar to the ones in the reference periods. During-Winds originating from the sectors southwest to south are usually below 6 m s^{-1} during days with densifica-

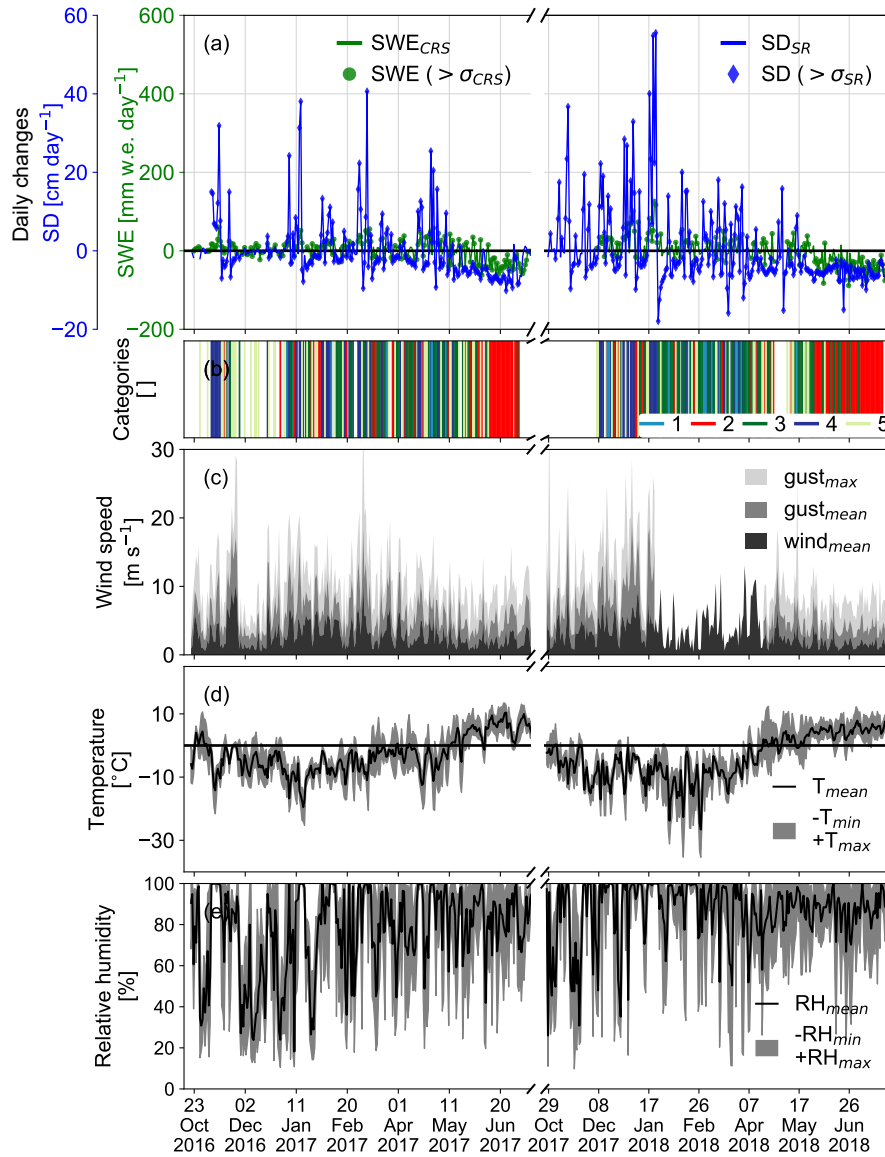


Figure 7. (a) Daily rates-changes of SD and SWE (green) and SD (blue). (b) Categorization of process-dominated days with 1 as accumulation, 2 as ablation, 3 as densification, 4 as accumulation with high confidence, and 5 as densification with accumulation (see Table 6). (c) Daily mean wind speeds (black shading), mean wind gusts (grey shading) and daily-maximum wind gust (dark light grey shading). (d) Daily mean temperature (black line) with daily-maximum and minimum temperature (grey shading). (e) Daily mean relative humidity (black line) with daily minimum and maximum relative humidity (grey shading).

tion, the wind direction is mostly. More frequently, however, the wind blows from south-east and is rather strong during the ablation days.

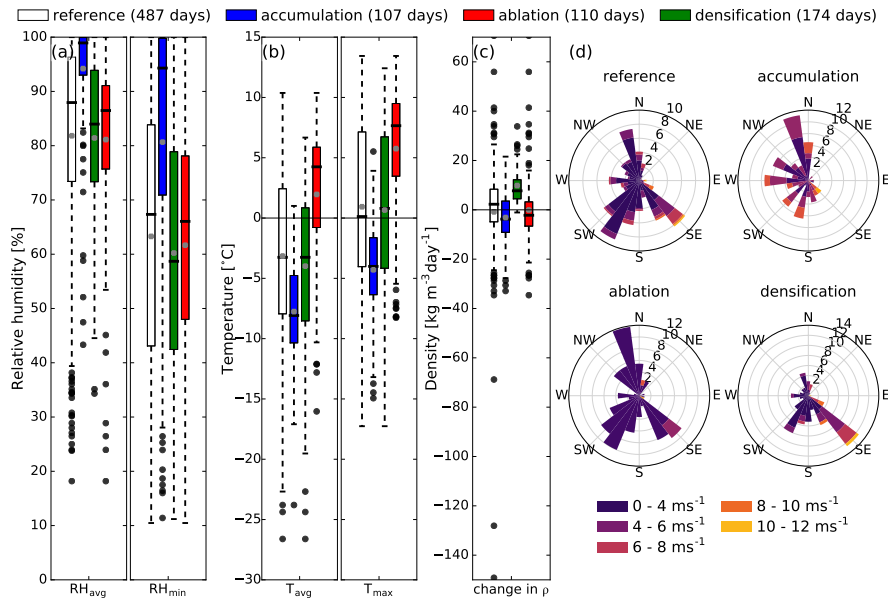


Figure 8. Summary of ~~daily values of the daily meteorological conditions during process-dominated days (accumulation, ablation and densification).~~ (a) ~~Daily~~ mean and minimum relative humidity, (ab) ~~-daily average-mean~~ and maximum temperature, (bc) ~~and~~ the change in mean bulk snow density, and (ed) ~~-The wind roses show~~ mean daily wind speeds ~~with wind direction (d) and -direction.~~ The numbers in the ~~wind~~ roses correspond to the percentage of days within that selection. The reference includes all days with valid data (487 days).

All these findings align with our general expectations that accumulation ~~happens-occurs~~ with lower temperatures, high relative humidity, and stronger winds. Ablation through melt is mainly characterized by higher temperatures, lower relative humidity and lower wind speeds. Of all densification days, ~~+143%~~ show a simultaneous increase in SWE ("densification with accumulation", Table 6). When both processes occur ~~during the one single day at the same day,~~ it suggests either simultaneous
5 compaction of snowfall, accumulation by ~~wind-snow~~ drift, or infiltration of liquid precipitation. About ~~one-third~~ ~~40%~~ of these days have ~~daily mean temperatures above 0 °C which suggest infiltration.~~ Another third of these days have ~~daily mean negative temperatures and low wind speeds, while the remaining 60% have either positive temperatures or~~ wind speeds above 4 m s^{-1} ; ~~which suggests wind drift.~~ The last third have ~~negative mean temperatures and wind speeds below 4 m s^{-1} .~~ ~~Positive daily temperature might suggest infiltration within the snowpack. Higher wind speeds would rather suggest an effect of snow drift.~~

10 4.3 ~~Comparison of snow accumulation to precipitation observations~~ ~~Precipitation scaling~~

~~The~~ ~~With the~~ daily observations of SWE ~~on Plaine Morte allow a comparison to daily precipitation sums from nearby weather stations at lower elevations and gridded precipitation (RhiresD)~~ we assess the accuracy of an approach utilizing scaled precipitation from three nearby AWS and RhiresD. In the following, we refer to the autonomous CRS measurements as

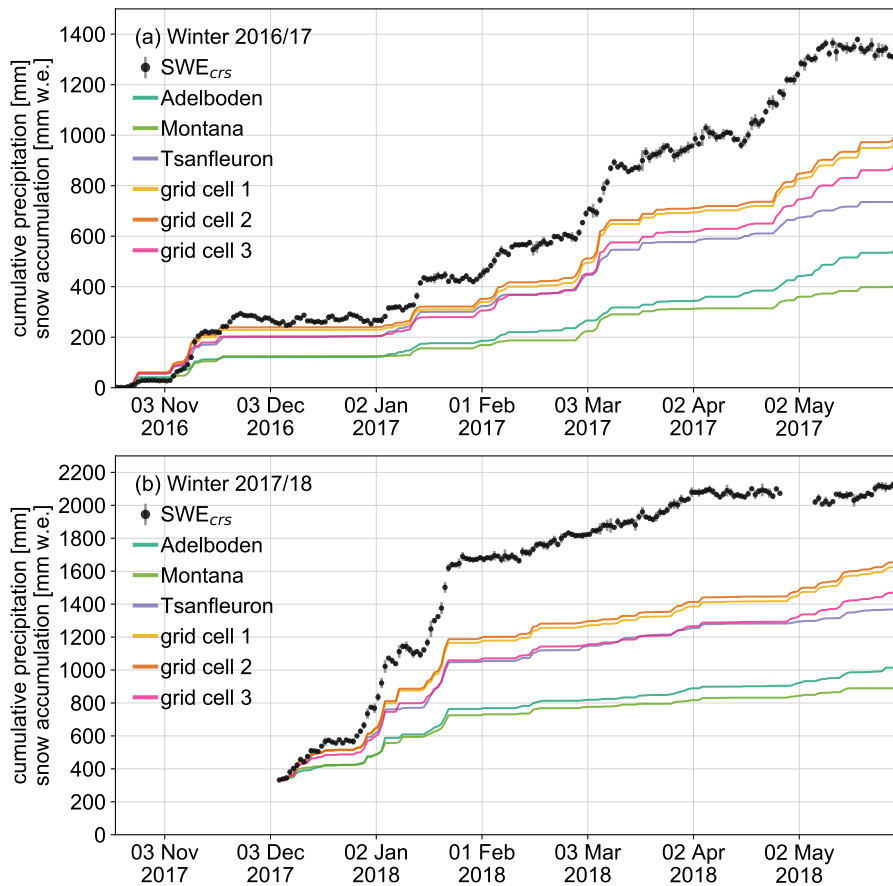


Figure 9. Cumulative precipitation and snow accumulation of (a) winter 2016/17 and (b) winter 2017/18. Black dots show daily SWE observations with their standard deviations. Colored lines represents all cumulative precipitation time series.

~~snow accumulation , and cumulative precipitation from other sources as precipitation sums. Cumulative precipitation and snow accumulation of (a) winter 2016/17 and (b) winter 2017/18. Black squares show the daily measured means with daily standard deviations of the SWE measurements. Cumulative precipitation is corrected with a constant bias to fit the beginning of measurements. or SWE.~~

- 5 ~~Fig. 9 shows the cumulative precipitation of three nearby stations at lower elevations, including Adelboden (1322 masl) and Montana (1427 masl, Table 2). In addition, cumulative precipitation from three grid cells of RhiresD are included (grid cells 1-3). As to be expected, precipitation sums are significantly lower than Without applying a scaling factor, we see a large difference between cumulative precipitation and snow accumulation on the glacier. This is mainly due to orographic effects but could also be caused by wind drift, (Fig. 9). This could be due to the high spatial variability of solid precipitation and/or~~
- 10 ~~undercatch of the rain gauge. rain gauges (Kochendorfer et al., 2017; Pollock et al., 2018).~~

Table 7. Scaling factors resulting in a minimal MAE. Two different approaches are presented; one factor applied and three factors applied distinguishing between the precipitation regimes (solid, mixed and liquid).

	one factor		three factors			
	all []	MAE [emmm w.e.]	solid []	mixed []	liquid []	MAE [emmm w.e.]
Adelboden	2.8	7.879 ± 5.755	2.9	1.8 1.3	0.2 0.6	4.141 ± 3.8 37
Montana	3.3	7.676 ± 4.3 42	3.4	3.4 2.5	0.2 0.8	5.656 ± 3.6 37
Tsanfleuron	1.8	7.170 ± 3.6 37	1.8	2.0 1.4	0.2 0.5	5.450 ± 2.5 29
grid cell 1	1.5	7.372 ± 4.4 43	1.5	1.2 0.9	0.1 0.3	4.748 ± 4.1 43
grid cell 2	1.4	7.474 ± 6.0 59	1.5	1.2 0.8	0.1 0.3	4.039 ± 2.8 30
grid cell 3	1.6 1.7	7.978 ± 7.1 43	1.7	1.3 0.9	0.1 0.3	4.646 ± 4.2 44

In general, the ~~timing of increases in onset of~~ snow accumulation corresponds well with increases in the precipitation observations. ~~Still, there are some exceptions as, for instance, in mid-~~However, in November/ beginning of December 2016 ~~increases in SWE are observed with no corresponding increase in precipitation registered at the AWS~~ (Fig. 9a). In addition, ~~during some time periods accumulation increases more strongly than precipitation-~~Montana captures fewer precipitation events ~~than other stations in winter 2016/17~~ (Fig. 9a). In winter 2017/18, Montana captures approximately the same number of events ~~as the other AWS~~ (e.g. mid-April 2017). During most of such time periods, daily mean wind speeds remain below 6 m s^{-1} . Mean daily wind gusts are mostly below 10 m s^{-1} (Fig. 7c). Nonetheless, wind drift cannot be excluded to locally increase snow accumulation.

In the second winter, it is evident that the sums during single precipitation events are lower than for snow accumulation. ~~This is the case until mid of January 2018. During most of December 2017, 9b). At times when SWE increases without an increase in precipitation~~ (e.g. December 2016, mid-February 2017 and mid-February 2018) we also observe higher mean daily wind speeds ~~are above 5 m s^{-1} and maximal wind gusts~~ (Fig. 7c). Thus, wind drift may cause these discrepancies. Our analysis of days dominated by accumulation (Fig. 8) shows that wind speeds are mostly higher 8 m s^{-1} and that the direction does not vary strongly during such days. This suggests an almost constant influence of wind drift. ~~This suggests snow drift as an explanatory mechanism.~~ Precipitation amounts are generally lower than SWE amounts observed for individual events on the glacier. This bias seems to increase with the duration of the precipitation events, especially for those lasting several days.

Using the continuous time series of snow accumulation on Plaine Morte, we determine the precipitation scaling factor for each weather station and grid cell which leads to a minimal MAE for the reproduced accumulation on the glacier over the two winter seasons. ~~The gridded precipitation has-~~ The optimal scaling factors range from 1.4 (grid cell 2) to 3.3 (Montana). ~~Gridded precipitation and Tsanfleuron have~~ similar scaling factors (Table 7). The ~~precipitation measured at Tsanfleuron has a~~ scaling factor in a similar range as for the grid-cells. The two stations which are located at elevations around 1400 m lower than the measurements at Plaine Morte, have scaling factors of ~~two AWS have significantly higher scaling factors with~~ 2.8 (Adelboden) and 3.3 (Montana). ~~Applying the given scaling factors, we can reproduce snow accumulation with a MAE of~~

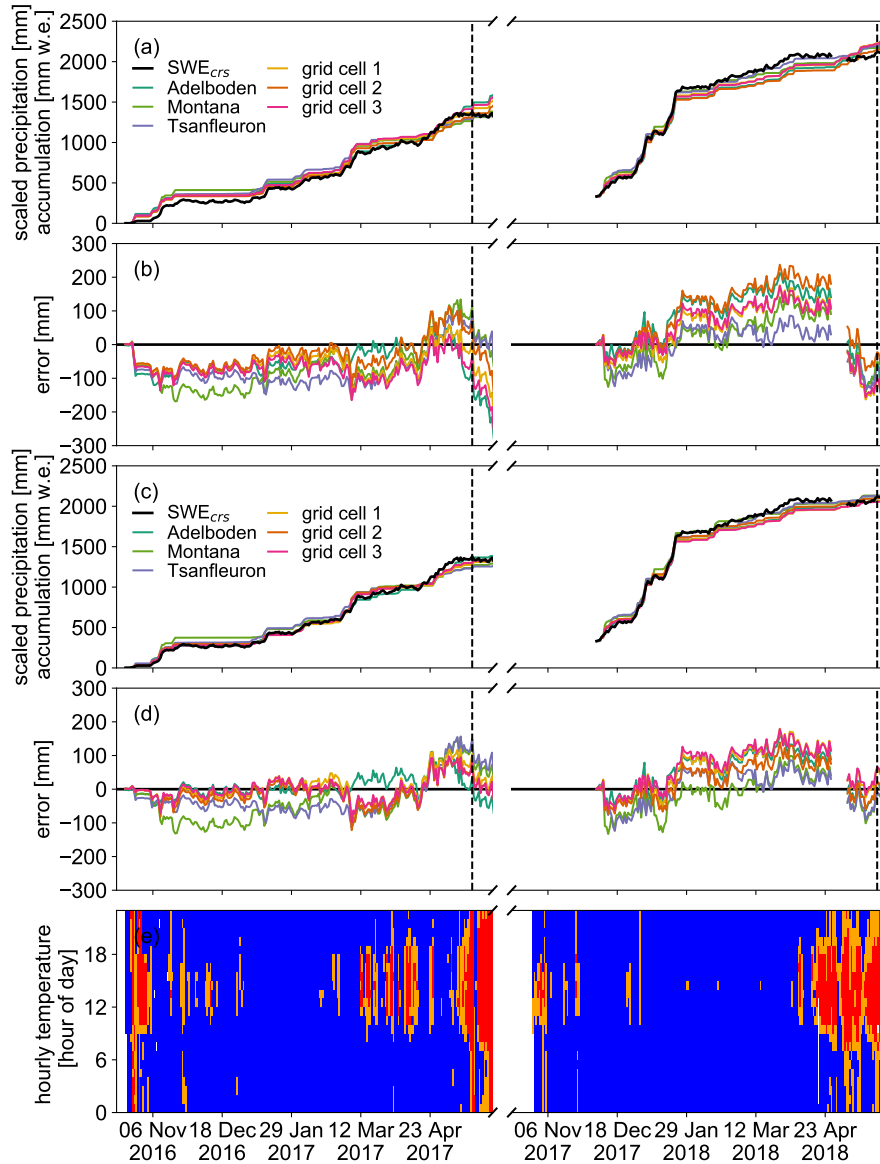


Figure 10. SWE observations (black dots) and scaled cumulative precipitation with (a) one factor and (c) three precipitation phase-dependent scaling factors (see Table 7). (b) and (d) show the difference between precipitation and SWE of (a) and (c), respectively. The hourly temperature at Plaine Morte is visualized in (e) with temperatures above 3°C colored in red, between 0°C and 3°C in orange, and below 0°C in blue. The dashed line corresponds to the date of the seasonal maximum in SWE.

~~below 8 cm w.e.~~The best performance is found for ~~the station at~~ Tsanfleuron with a MAE of 7.170 ± 3.6 cm. ~~We find that accumulation 37 mm w.e.~~

Accumulation events in October/ November 2016 ~~are not well reproduced by the scaled weather station precipitations;~~ ~~accumulation~~ and May 2017 are represented fairly poorly by precipitation observed at AWS. Accumulation is overestimated by at least 5 cm 50 mm w.e. (Fig. 10a ~~and b~~). ~~The same observation has been made for May 2017.~~ In these months, hourly temperatures at Plaine Morte ~~can~~ reach values higher than 0°C (Fig. 10e). It is thus likely that precipitation falls in its liquid form ~~rather than solid as rain rather than snow~~. Nonetheless, it may still contribute to the SWE by refreezing. ~~However, this effect is only relevant within an~~, a process that would only be relevant in isothermal snowpack. (a) ~~Time series of the scaled cumulative precipitation with one factor per station. Brackets show the best scaling factor for the time series. (b) shows the difference between the precipitation and accumulation with their mean absolute error and standard deviation given in the label. (c) shows the time series scaled for the different temperature regimes. The scaling factor is given in brackets (solid/mixed-phase/liquid).~~ (d) is the same as in (b), just for the temperature scaling regimes. (e) The hourly temperature at Plaine Morte indicating temperatures above 3°C (red), between 0°C and 3°C (orange), and below 0°C (blue).

With the applied distinction of the precipitation phase, we find The temperature-dependent parameterization for the precipitation phases result in potentially 68 days (17%) with liquid precipitation, 288 days (72%) with solid precipitation, and 46 days (11%) where precipitation is most likely a mixture between solid and liquid precipitation. For each of these precipitation regimes, we derive an optimal scaling factor for each station (Table 7) and calculate snow accumulation (Fig 10e) with mixed-phase precipitation. Table 7 provides the resulting optimal scaling factors for each of these phases. The scaling ~~factor~~ factors for solid precipitation remains similar to the ~~ones for the whole time series first analysis~~ (Fig. 10a). Mixed-phase precipitation is scaled by slightly and liquid precipitation are scaled by lower factors. Liquid precipitation, however, shows factors smaller Scaling factors for liquid precipitation are smaller than a factor of one (Table 7). With these scaling factors ~~we can~~, we reduce the MAE ~~of precipitation to snow accumulation to below 6 cm to below 60 mm w.e.~~ With the newly scaled time series and the temporal evolution is generally consistent with the SWE observations on the glacier (Fig. 10c), ~~the reproduction of snow accumulation through precipitation observations is improved. It especially affects the beginning of winter 2016/17 and the end of May 2017/18. After the accumulation-phase correction, grid cell 2 has the lowest MAE with 4.0 ± 2.8 cm. This grid cell is directly located above the station at Plaine Morte. The station in the south of the glacier, Montana, has the lowest performance with a MAE of 5.6 ± 3.6 cm.~~

5 Discussion

5.1 ~~Instrument~~ CRS performance and limitations

In this study, we used a CRS in combination with a sonic ranging device to measure and compare snow accumulation over two winter seasons. ~~The evaluation~~ The CRS shows a good agreement with manual field measurements ~~showed an average overestimation of~~. On average, the CRS overestimates SWE by +2% of SWE values by the CRS. We found that the manual field measurements carry a higher uncertainty than the autonomous CRS measurements of SWE. By taking this uncertainty into consideration, we suggest that SWE observed by the CRS lies $\pm 13\%$. The agreement of the individual field campaigns varies between an excellent agreement within $\pm 2\%$ (10 May 2017 and 19 December 2017) and a rather large

~~difference of more than $\pm 20\%$ (27 March 2017 and 10 January 2018). Otherwise, the agreement is within the uncertainty range of the manual measurements (Fig. 6a). However, during two field campaigns (27.03.2017 and 10.01.2018) the difference between automated and manual measurements of SWE exceeds 20%. The SD measurements are also under- and overestimated by more than 5%, resulting in a difference larger 10% of the bulk snow density. Possible explanations can be attributed either to the field observations or to the CRS measurements. There might have been errors introduced when obtaining the field data. Another possibility is a potential problem in the calculation of SWE from neutron counts at SWE values between 90 and 120 cm. Furthermore, a spatial bias may be introduced: snow pits have never been dug directly above the CRS because of their destructive nature. In fact, it is field measurements.~~

~~In the second winter season, SWE amounts were exceptionally high with more than 2000 mm w.e. Nevertheless, the most likely explanation for discrepancies in seven of nine field surveys: agreement to field measurement is within $\pm 10\%$ indicating that the measurement limit of SWE has not yet been reached. Due to the exponential nature of the relationship there is no distinct threshold beyond which the relative neutron count is no longer sensitive to SWE (Fig. 2).~~

~~The SWE calculations from neutron counts are not too sensitive to the initial count rate N_0 when SWE is greater than approximately 40 cm. For SWE values above 40 cm, it hardly influences resulting SWE values due to data processing of the neutron counts as presented is straightforward. Given the transformation equation, only the initial neutron count rate can be calibrated. But a variation of this calibration parameter within its uncertainties has little influence on the resulting SWE amounts, especially for amounts larger 400 mm w.e. This is a consequence of the exponential nature of the conversion equation (Eq. 5). Moreover, the calculated SWE fluctuates between -0.5 cm and 0.5 cm during snow-free conditions. We take this into account by adding an additional uncertainty in Eq. ??~~ More importantly, the neutron count rate may also be influenced by how we correct for air pressure and solar activity even though we apply the same equations as presented in previous studies for SWE (e.g. Howat et al., 2018) or soil moisture studies (e.g. Zreda et al., 2012; Andreasen et al., 2017). In contrast to previous studies of above-ground CRS, we do not correct for the changes in atmospheric moisture. We assume that for the below-ground CRS, fast neutrons are produced within the snowpack rather than in the atmosphere, an assumption also made in Howat et al. (2018), and implicitly made by preceding authors in their studies (e.g. Kodama et al., 1979; Paquet and Laval, 2005; Gottardi et al., 2013). Another source of uncertainty is the semi-empirical fit that has been used in this study. Because our study focuses on the application for snow and glacier studies, we have chosen to apply the relations used by Howat et al. (2018). In general, the uncertainty estimate presented here is rather generous. The straightforward and robust data processing is one of the advantages of the CRS conversion function has the potential to introduce considerable uncertainty in the inferred SWE. However, the applied empirical relation has shown to be adequate as the resulting SWE agrees well with independent field measurements, indicating only a minor bias and a standard deviation for individual observations that lie in the range of the uncertainty of the in situ SWE surveys.

~~Directly comparable to our study is the~~ For all correction factors such as air pressure and solar activity, we propagated an estimated uncertainty through all equations and show that the precision is mainly defined over the neutron count rate. Assuming that the parameterization of the correction equations carry no uncertainties, the influences of all other measurements and constant parameters are small. Moreover, an independent study by Howat et al. (2018) , where they deployed a CRS on

the Greenland quantified a precision of 0.7% of a CRS lying below the snowpack on the ice sheet. With the variability of SWE estimations, they define a precision of 0.7%. This precision is significantly lower than our uncertainty range. Generally higher neutron counts and lower SWE values place Howat et al. (2018) on a steeper. Their results, however, are affected by lower in situ air pressure and consequently higher neutron count rate. In addition, Howat et al. (2018) observed lower SWE amounts which places them on a steeper part of the calibration curve which results in more precise results. The level of noise is also lower at higher neutron counts. In our study, we define the uncertainty range such that it includes the noisiness of the neutron counts. In addition, we integrate the temporal resolution to daily values because of the noise. Overall, the noise levels can be reduced by either integrating the neutron counts over a longer time period or by adding more neutron detectors. In the latter case, however, it becomes quite costly. (Fig. 2). For lower SWE amounts, changes in neutron counts are more sensitive and have a higher precision. The precision can be increased by integrating over longer time periods.

In general, one could argue that a snow scale or snow pillow would have been more suitable for such an analysis, especially given the higher temporal resolution during the accumulation phase. However, such devices are not well suited for this site because of the surface roughness of the glacier, the lack of a large flat surface and the changing surface by ice melt. In addition, ice bridging would have been problematic. For sub-snow GPS, one problem might be the glacier movements or the surface melt. In addition, data processing is different for dry or wet snow and is therefore more complicated.

The main advantage of the CRS is that it can be deployed in an exceptionally wide variety of terrain. There is no need for a stable and flat surface nor does it depend on the reception of satellite signal for its measurements (cf. Section 1.1). The correction factors for air pressure and solar activity can easily be interpolated. Air pressure can be measured in situ without the need of an elaborate measurement setup. These advantages, however, only apply when we are solely interested in SWE observations. As soon as further observations such as SD or other meteorological parameters are required, the potential deployment areas become more limited.

5.2 Evolution of snow density

The snowpack of the presented winters here two winters that we studied evolved differently in terms of amounts and accumulation rates. Simultaneously However, the evolution of the mean density of the snowpack is very alike similar between the two winter seasons. The evolution before the onset of melt agrees well with the findings of Mizukami and Perica (2008). However, and Saito et al. (2012). But snow densities become quite high ($>600 \text{ kg} \cdot \text{m}^{-3}$) during the melt season in our study. Saito et al. (2012) present similar graphs as to Fig. 5. Nevertheless, mean densities after After the SD maxima snow densities did not exceed $500 \text{ kg} \cdot \text{m}^{-3}$. Another study conducted in Saito et al. (2012). A study in the Austrian Alps by Schattan et al. (2017) also shows lower mean snow densities towards the end of the snowpack. Schattan et al. (2017) argue that the surrounding patchy snow distribution biases the point-scale measurements of SWE. Even though they used an above ground CRS, which provides a larger sampling area, the CRS setup of our study may also be affected by such influences. Many effects may lead to high densities; water-saturated snow. The high snow densities presented here could be a result of changes in the snow physics, measurement errors of SWE and SD estimations (Eq. 7), or a combination of both. Physical changes within the snowpack could be due refreezing of liquid water at several layers within the snowpack, water saturated snow in the top layers,

locally thick ice lenses, or accumulation of liquid water around the CRS which eventually refreezes. With the CRS and the SR, we can only determine a mean snow density. Therefore, not all these effects would be identifiable, and explanations remain speculative. Despite all potential explanation for errors by the CRS, it could also be a problem with the SD measurements rather than the SWE measurements.

5 ~~In our study setup, several reasons could cause erroneous SD measurements. Firstly~~

SWE from the CRS could, for example, be affected by a suprafacial pond in the vicinity of the site. It remains unclear how such a hydrogen pool would influence the in situ point measurements of the below-ground CRS. Other influences could come from the correction factors of the neutron count rate or the conversion equation applied in this study (cf. Section 5.1).

The SD measurements are also susceptible to errors. For example, the snow area below the sonic ranging sensor may show a small depression because of wind turbulence caused by the mast. ~~Furthermore~~Additionally, the snow around the ~~metal mast~~ main pole of the station melts faster possibly leading to a depression ~~with a larger radius around the mast~~. It remains difficult to assess whether the radius of this depression would be within the footprint of the sonic ranging sensor. ~~Nevertheless, these two effects may superimpose. Secondly~~In winter 2017/18, the solar panels were submerged below the snow. To ensure further power supply, we had to ~~free the solar panels by digging a dig them out. This~~ snow pit around the ~~mast in winter 2017/18. This snow~~ pit main pole would have been refilled by wind, but densities are different, probably causing accelerated melt rates around the mast. ~~Thirdly, the influences~~For more shallow snowpacks, the metal anchorage of the mast's foundations ~~, the wooden beams with the metal anchorage, may cause erroneous SD measurements for more shallow snowpacks. This also becomes clear since SD measurements never reach~~ might interfere with the SD measurements. The SD measurements, for instance, never observe a SD of 0 cm even though the sensor is calibrated for the mounted height and agreements to snow probings agree during the ~~season (Fig. 4)-b and Fig. 6).~~

In summary, this study setup shows that we are able to gain important information concerning the temporal evolution of snow density. We are able to derive the main periods of snow accumulation, densification and melt and it seems to follow a consistent pattern over two winter seasons (Fig. 5). In that sense, the CRS does not distinguish between water, snow and ice which avoids a falsification of SWE estimates. But it also becomes impossible to determine the snow layering. The SD observations seem to be more sensitive during the melting phase, probably because of the small-scaled heterogeneity in snow melt.

5.3 Comparing observed snow accumulation to precipitation observations

5.3 Estimating snow accumulation by precipitation scaling

~~We directly compared measured snow accumulation to precipitation sums of nearby stations and grid cells of RhiresD. With this comparison, we aimed at reproducing snow accumulation by using surrounding stations with precipitation measurements. Precipitations sums which are taken from the nearby weather stations are expected to show lower accumulation amounts. Wind drift, orographic effects, different temperature regimes, etc. lead to higher amounts of snow accumulation than precipitation sums~~The comparison of snow accumulation to precipitation observations is not without caveats given that snow accumulation

is cumulative while precipitation is instantaneous. Moreover, snow accumulation is influenced by precipitation, snow drift and evaporation whereas precipitation is not. When continuous SWE measurements are unavailable, a straightforward and simple approach is to use precipitation data scaled to a ground reference. In the case of RhiresD, the spatial resolution of 1×1 km does not suffice for the complex topography. In reality, the measurement site is at a higher elevation than in RhiresD, and may therefore lead to precipitation sums that are too low. The glacier-wide mass balance studies on Plaine Morte this approach is applied using precipitation observations from Montana (GLAMOS, 2018). Precipitation data from AWS or RhiresD is freely available and highly resolved which makes it widely applicable. A drawback for AWS stations is the potentially large undercatch of solid precipitation combined with high wind speeds which can be on the order of a factor of three given solid precipitation and high wind speeds (Kochendorfer et al., 2017). The gridded precipitation, RhiresD, is potentially influenced by measurement errors as well as an underrepresentation of observations at high elevations. In addition, the complex topography of mountainous terrain is typically not sufficiently resolved in gridded data products.

Despite all caveats, we are able to reproduce the evolution of snow accumulation with a MAE below 8 cm. The seasonal evolution of both winters could be reproduced with a constant factor between 1.4 and 3.3 for the AWS and RhiresD (Fig. 10 and Table 7). The minimal MAE is below 80 mm w.e. and with a standard deviation of below 8 cm, with larger absolute discrepancies during the second winter season (Fig. 10b). In practice only a snapshot of SWE is available to scale precipitation data and thus the error at the daily resolution is most likely higher.

Applying a precipitation-phase-dependent scaling factor reduces the MAE to below 60 mm w.e. This MAE is in the same range for all compared stations. With the information of temperature at Plaine Morte, we can even improve the scaling of precipitation. For solid precipitation, the factor is almost the same. The main improvement occurs during days where temperatures are > 0 °C. The phase of precipitation is parameterized using air temperature at the glacier site. Since air temperature is not as spatially heterogeneous as precipitation it can be interpolated with less uncertainties. The parameterization proposed here distinguishes the precipitation phase between three temperature thresholds: below 0 °C, between 0 °C and 3 °C and above 3 °C during at least six hours. During such days, precipitation adds little to the snowpack. Nonetheless, we would still expect an increase in SWE at deeper snowpacks due to the refreezing process. Several reasons could explain why we do not see this behavior; Firstly, the CRS might not be able to capture water infiltration because of its noise levels from April to May, where SWE values are above 100 cm w.e. Water infiltrated within the snowpack may refreeze at a different location due to lateral transport. For instance, a superficial pond of water close to the mast installation was observed in the field campaign of May 2018. Not many devices would be able to capture such a process automatically. Liquid water that penetrates the whole snowpack and refreezes below the sensor is not registered by the sensor. Secondly, some of the precipitation at Adelboden in May 2018, It is in line with previous studies. (Jennings et al., 2018), for example, determined a snow-rain threshold between -0.4 °C and 2.4 °C in the Northern Hemisphere.

The scaling factor for the solid phase remains similar to the overall constant factor because most precipitation falls in its solid form during the winter season. Mixed-phase precipitation is scaled with lower factors while liquid precipitation has scaling factors below one. Especially for liquid precipitation, we observe a seasonal component. Liquid precipitation occurs mainly at the beginning and ending of the winter season (Fig. 10e). For winter 2016/17, for instance, resulted from thunderstorms. These

amounts have a short, but high peak and may not have occurred in the first precipitation event does not result in accumulated snow and therefore the constant scaling factor overestimates the beginning (Fig. 10b). At the end of the same intensity on the glacier. Thus, precipitation amounts would be smaller on the glacier. Fourthly, the infiltration of water into the winter seasons, the snowpack is around its maximum and liquid precipitation would infiltrate the snowpack would warm the top layers of the snowpack by latent heat release of the refreezing water. Consequently, faster melt rates would be favored after the precipitation event. Independently, sublimation could also occur beforehand. With the daily resolution, such processes cannot be identified as we need a sub-daily resolution. But at higher temporal resolutions, noise levels of the CRS would override signals within the deep snowpack. If we only consider changes in SD, such as the accumulation days defined in Table 6, no increases in SD occur from mid of May to end of May (Fig. 7b). During this period, most precipitation events are classified as either liquid or and refreeze contributing to an increase in SWE. To avoid liquid and mixed-phase. From mid of March to mid of April 2017, some accumulation events result in increases of SD below 10 cm. These events do not have a signal in the SWE measurements precipitation, the time period in which precipitation is accumulated could be adjusted. However, an adjustment of the time period would only partly exclude such events.

The choice of the precipitation data and AWS is also important. RhiresD has shown a better performance especially for the phase-dependent scaling factors. Tsanfleuron (2052 m a.s.l.) has the lowest constant factor (1.8) and MAE (70 ± 37 mm w.e., Table 7) for the phase-independent approach. Adelboden and Montana which are located north and south of Plaine Morte have higher scaling factors than Tsanfleuron. In addition, they are on either side of the Alpine ridge and dominated by different weather regimes which is also confirmed by analyzing the temporal evolution. In winter 2016/17, many events captured by Adelboden are not represented in Montana (Fig. 79a). Nonetheless, Montana does not perform worse than Adelboden with only one constant factor. In the case of the phase-dependent scaling, the performance of Adelboden is significantly improved reducing its MAE by almost a factor of two.

Another uncertainty is introduced by the temperature thresholds applied in this approach. Previous studies have shown that the snow-rain threshold varies on a global scale between -0.4°C and 2.4°C in the Northern Hemisphere (e.g. Jennings et al., 2018). To refine the temperature thresholds, we need a higher temporal resolution of SWE measurements. For the SD observations, we have an hourly resolution. Given that precipitation falls in its liquid form, it would not be as an increase in snow accumulation but as a decrease. Our calculation was possible only because we had reliable and continuous snow accumulation data. Because the spatial variability of snow accumulation on Plaine Morte is rather low the analysis can be made with a point measurement as a reference. But at high mountain sites with more topographic gradients, the location of the in situ measurement becomes more important which is why a glacier-wide mean is typically used. Another caveat of this assessment is the uncertainty of the CRS measurements which has not been taken into consideration. Nonetheless, the resulting MAE lie within $\pm 13\%$ of the average agreement between CRS and within the uncertainty of manual measurements.

In summary, it is possible to infer the temporal dynamics of snow accumulation at a high-elevation site by means of scaled precipitation data. However, at least one in situ observation is required for applying this approach. The choice of the precipitation data series and the time period considered is crucial for this methodology.

6 Conclusions and perspectives

During two winter seasons, we ~~measured~~ observed snow accumulation and ablation on a Swiss glacier at a daily resolution. The ~~installed CRS showed good performance in comparison to in-situ observations with an average overestimation of the SWE of deployed CRS withstood the harsh environmental conditions at the high mountain site and measured reliably. The validation~~
5 ~~with manual field measurements indicated a mean accuracy of $+2\% \pm 12\%$. The mean densities from CRS observation obtained with combination with a sonic ranger agreed with a standard deviation 13%. In combination with continuous SD measurements, the CRS provided daily mean snow densities that were within a range of $\pm 8\%$ on average. With this data, we could show of manual in situ snow density surveys.~~

With the daily mean snow density observations, we showed that the evolution of the bulk snow density ~~was quite similar~~
10 ~~for two very different winter seasons. We investigated environmental conditions that led to changes in the snowpack can be divided into three main periods; accumulation, densification and ablation. Throughout the accumulation period, snow densities are low with periodical repetitions of snowfall and subsequent densification. At the seasonal maximum of SWE the snowpack densifies during several days before its melting period begins. Additionally, we investigated these three processes at a daily resolution. Days with accumulation, ablation and densification could be attributed to days with specific prevailing~~
15 ~~meteorological conditions at this site basis and could attribute general meteorological conditions to each process.~~

The ~~availability of snow accumulation at daily resolution allows the direct comparison of high-elevation accumulation with precipitation of nearby stations at lower elevations. Optimal scaling factors were evaluated for different stations and grid cells of Rhires~~
20 ~~Deployment of the CRS on Plaine Morte provided continuous observations of SWE that could be used to assess the optimal scaling factor for readily available precipitation data. With the scaling factors, the snow accumulation could be reproduced optimal scaling factor, we were able to obtain snow accumulation with a MAE below 8 cm. Taking temperature into account, the MAE could be further reduced to below 6 cm. Even though the approach of scaling precipitation to snow accumulation is strongly simplified, it is effective for reproducing the evolution of snow accumulation at a daily resolution of below 80 mm w.e. However, the performance depends on the choice of precipitation data, the choice of AWS, the date of the manual ground measurement and the time period considered. Scaling precipitation with a phase-dependent factor further~~
25 ~~improves these results.~~

In summary, we conclude that the CRS is ~~so far the most suitable measurement device for measuring SWE continuous~~
30 ~~a highly promising device for observing SWE continuously in~~ cryospheric high alpine environments. Despite its limitations through the level of noise ~~, and its high uncertainties in a deeper snowpack and its precision depending on absolute snow amounts~~, it is suitable for long-term monitoring of SWE in ~~high-mountain high mountain~~ regions as well as polar regions. In such areas, its ~~robustness resilience~~ in harsh environmental conditions, its rare need for maintenance (once it is properly running) ~~, its little demands and its flexibility~~ regarding site topography ~~and its straightforward data processing with little sensitivities to input parameters make it an ideal device for continuous SWE measurements. For more shallow are convincing. For shallower~~ snowpacks, the temporal resolution can be increased to a sub-daily scale. ~~Concerning a financial aspect, the sensor itself lies in the cost range of other devices for SWE observations. The presented measurement installation is costly. For~~

long-term monitoring of SWE, such an extensive installation. For this study, we chose an elaborate measurement setup which would not be necessary if only SWE measurements are required.

Future studies could analyze the spatial footprint of a CRS lying below the snowpack. Furthermore, spatial distribution of continuous SWE measurements would allow further understanding of the spatial variability in snow accumulation, solid precipitation, precipitation phases and its relation to snow accumulation. In future, the point-scale footprint of the CRS should be better investigated by modelling of neutron trajectories. It would be particularly important to better quantify the influence of hydrogen pools in close vicinity of a subsurface CRS. More investigations into the location-dependent correction of the solar activity would provide further insights into the applied processing of raw neutron counts. The deployment of additional CRS observations in other high-mountain regions of the Alps would not only give further indications on the suitability of precipitation scaling but also the spatial variability of snow accumulation.

Data availability. All observations at the Glacier de la Plaine Morte are available upon request from the first author. In future, it will also be available in an online repository.

7 Correcting raw neutron counts

The correction of the raw neutron counts (N_{raw}) to account for in-situ influences has been presented in previous studies (Zreda et al., 2012; Sigouin and Si, 2016; Andreassen et al., 2017; Howat et al., 2018). In this study, we apply the same equations. The neutron counts of the CRS are corrected with the solar activity (F_s) and the in-situ air pressure (F_p , Eq. ??).

$$N = N_{\text{raw}} \cdot F_s \cdot F_p$$

The correction factor F_i is determined as

$$F_s = 1 + \beta \cdot (F_{\text{sol}} - 1)$$

The variable F_{sol} represents the 13-hour centered rolling mean of the neutron counts at Jungfraujoch (JUNG) divided by the hourly neutron count values. The unit less scaling parameter β , provided by the manufacturer, is 0.95 in this study. It has been determined by the location of the mast installation at Plaine Morte (46.4N, 7.5E, 2700 m) relative to the neutron monitor station at Jungfraujoch (Fig. 1). The other correction factor, the pressure factor, is calculated as

$$F_p = \exp\left(\frac{p - p_0}{L}\right)$$

The attenuation length L is assumed to be 132 hPa. The hourly pressure values are represented by p , and p_0 stands for an arbitrarily chosen pressure reference (739 hPa).

Author contributions. RG prepared the manuscript, performed field work and data analysis with contributions from all co-authors. NS and MH contributed to the design and execution of the study. DD gave essential inputs on how to process the output of the cosmic ray sensor and define its measurement uncertainty.

Competing interests. Authors RG, NS and MH declare that they have no competing interests. Author DD is the owner of Hydroinnova LLC.

- 5 *Acknowledgements.* This study is supported by the Swiss National Science Foundation (SNSF), grant 200021_178963. MeteoSwiss provided the data of all stations besides the one at Plaine Morte. Jungfrauoch neutron monitor data were kindly provided by the Cosmic Ray Group, Physikalisches Institut, University of Bern, Switzerland. We like to thank H. Gubler from ALPUG, W. Jäger from WALJAG and T. Sarbach from Sarbach Mechanik GmbH. They designed the mast, programmed the logger box, and helped with the field installation. Furthermore, we like to acknowledge all the field helpers during the two winter seasons. Without them, this study would not have been possible. Last but
- 10 not least, we thank the two anonymous reviewers for their detailed and constructive feedback.

References

- Ali, S. A., Aadhar, S., Shah, H. L., and Mishra, V.: Projected Increase in Hydropower Production in India under Climate Change, *Scientific Reports*, 8, 12 450, 10.1038/s41598-018-30489-4, 2018.
- Andreasen, M., Jensen, K. H., Desilets, D., Franz, T. E., Zreda, M., Bogena, H. R., and Looms, M. C.: Status and Perspectives on the
5 Cosmic-Ray Neutron Method for Soil Moisture Estimation and Other Environmental Science Applications, *Vadose Zone Journal*, 16, 0, <https://doi.org/10.2136/vzj2017.04.0086>, 2017.
- Barnett, T. P., Adam, J. C., and Lettenmaier, D. P.: Potential impacts of a warming climate on water availability in snow-dominated regions, *Nature*, 438, 303–309, <https://doi.org/10.1038/nature04141>, 2005.
- Campbell Scientific, I.: Instruction Manual SR50A, SR50A-316SS and SR50AH Sonic Ranging Sensors, revision: 10/16 edn., <https://s.campbellsci.com/documents/us/manuals/sr50a.pdf>, 2016.
10
- Castebrunet, H., Eckert, N., Giraud, G., Durand, Y., and Morin, S.: Projected changes of snow conditions and avalanche activity in a warming climate: The French Alps over the 2020-2050 and 2070-2100 periods, *Cryosphere*, 8, 1673–1697, <https://doi.org/10.5194/tc-8-1673-2014>, 2014.
- Clifford, D.: Global estimates of snow water equivalent from passive microwave instruments: History, challenges and future developments, *International Journal of Remote Sensing*, 31, 3707–3726, <https://doi.org/10.1080/01431161.2010.483482>, 2010.
15
- Cogley, J., Hock, R., Rasmussen, L., Arendt, A., Bauder, A., Braithwaite, R., Jansson, P., Kaser, G., Möller, M., Nicholson, L., and Zemp, M.: Glossary of Glacier Mass Balance and Related Terms, IHP-VII Technical Documents in Hydrology No. 86, IACS Contribution No. 2, UNESCO-IHP, Paris, 2011.
- Desilets, D., Zreda, M., and Prabu, T.: Extended scaling factors for in situ cosmogenic nuclides: New measurements at low latitude, *Earth and Planetary Science Letters*, 246, 265–276, <https://doi.org/10.1016/j.epsl.2006.03.051>, 2006.
20
- Desilets, D., Zreda, M., and Ferré, T. P.: Nature’s neutron probe: Land surface hydrology at an elusive scale with cosmic rays, *Water Resources Research*, 46, 1–7, <https://doi.org/10.1029/2009WR008726>, 2010.
- Dietz, A. J., Kuenzer, C., Gessner, U., and Dech, S.: Remote sensing of snow - a review of available methods, *International Journal of Remote Sensing*, 33, 4094–4134, <https://doi.org/10.1080/01431161.2011.640964>, 2012.
- Efthymiadis, D., Jones, P. D., Briffa, K. R., Auer, I., Böhm, R., Schöner, W., Frei, C., and Schmidli, J.: Construction of a 10-min-
25 gridded precipitation data set for the Greater Alpine Region for 1800-2003, *Journal of Geophysical Research Atmospheres*, 111, 1–22, <https://doi.org/10.1029/2005JD006120>, 2006.
- Egli, L., Jonas, T., and Meister, R.: Comparison of different automatic methods for estimating snow water equivalent, *Cold Regions Science and Technology*, 57, 107–115, <https://doi.org/10.1016/j.coldregions.2009.02.008>, 2009.
- Fierz, C., Armstrong, R., Durand, Y., Etchevers, P., Greene, E., McClung, D., Nishimura, K., Satyawali, P., and Sokratov, S.: The international
30 classification for seasonal snow on the ground, IHP-VII Technical Documents in Hydrology No. 83, IACS Contribution No. 1, UNESCO-IHP, Paris, 2009.
- Fischer, M., Huss, M., Barboux, C., and Hoelzle, M.: The new Swiss Glacier Inventory SGI2010: relevance of using high-resolution source data in areas dominated by very small glaciers, *Arctic, Antarctic, and Alpine Research*, 46, 933–945, <https://doi.org/10.1657/1938-4246-46.4.933>, 2014.
35
- GLAMOS: The Swiss Glaciers 1880-2016/17, *Glaciological Reports No 1-138*, Yearbooks of the Cryospheric Commission of the Swiss Academy of Sciences (SCNAT), published since 1964 by VAW/ ETH Zurich, https://doi.org/10.18752/glrep_series, 1881-2018.

- GLAMOS: The Swiss Glaciers 2013/14-2014/15, Glaciological Reports No 135-136, Yearbooks of the Cryospheric Commission of the Swiss Academy of Sciences (SCNAT), published since 1964 by VAW/ ETH Zurich, https://doi.org/10.18752/glrep_135-136, 2017.
- GLAMOS: The Swiss Glaciers 2015/16-2016/17, Glaciological Reports No 137-138, Yearbooks of the Cryospheric Commission of the Swiss Academy of Sciences (SCNAT), published since 1964 by VAW/ ETH Zurich, https://doi.org/10.18752/glrep_137-138, 2018.
- 5 Goodison, B. E., Louie, P., and Yang, D.: WMO solid precipitation measurement intercomparison, Tech. Rep. 67, World Meteorological Organization, 1998.
- Gottardi, F., Carrier, P., Paquet, E., and Laval, M.-T.: Le NRC: une décennie de mesures de l'équivalent en eau du manteau neigeux dans les massifs montagneux français, *International Snow Science Workshop 2013*, 33, 926–930, 2013.
- Hawdon, A., McJannet, D., and Wallace, J.: Calibration and correction procedures for cosmic-ray neutron soil moisture probes located across Australia, *Water Resources Research*, 50, 5029–5043, <https://doi.org/10.1002/2013WR015138>. Received, 2014.
- 10 Heilig, A., Schneebeli, M., and Eisen, O.: Upward-looking ground-penetrating radar for monitoring snowpack stratigraphy, *Cold Regions Science and Technology*, 59, 152–162, <https://doi.org/10.1016/j.coldregions.2009.07.008>, 2009.
- Heilig, A., Eisen, O., and Schneebeli, M.: Temporal observations of a seasonal snowpack using upward-looking GPR, *Hydrological Processes*, 24, 3133–3145, <https://doi.org/10.1002/hyp.7749>, 2010.
- 15 Henkel, P., Koch, F., Appel, F., Bach, H., and Prasch, M.: Snow Water Equivalent of Dry Snow Derived From GNSS Carrier Phases, *IEEE transactions on geoscience and remote sensing*, 56, 3561–3572, <https://doi.org/10.1109/TGRS.2018.2802494>, 2018.
- Hill, D. F., Burakowski, E. A., Crumley, R. L., Keon, J., Hu, J. M., Arendt, A. A., Wikstrom Jones, K., and Wolken, G. J.: Converting snow depth to snow water equivalent using climatological variables, *The Cryosphere*, 13, 1767–1784, <https://doi.org/10.5194/tc-13-1767-2019>, <https://www.the-cryosphere.net/13/1767/2019/>, 2019.
- 20 Howat, I. M., De La Peña, S., Desilets, D., and Womack, G.: Autonomous ice sheet surface mass balance measurements from cosmic rays, *Cryosphere*, 12, 2099–2108, <https://doi.org/10.5194/tc-12-2099-2018>, 2018.
- Huss, M., Bauder, A., and Funk, M.: Homogenization of long-term mass-balance time series, *Annals of Glaciology*, 50, 198–206, <https://doi.org/10.3189/172756409787769627>, 2009.
- Huss, M., Voinesco, A., and Hoelzle, M.: Implications of climate change on Glacier de la Plaine Morte, Switzerland, *Geographica Helvetica*, 25 68, 227–237, <https://doi.org/10.5194/gh-68-227-2013>, 2013.
- Huss, M., Dhulst, L., and Bauder, A.: New long-term mass-balance series for the Swiss Alps, *Journal of Glaciology*, 61, 551–562, <https://doi.org/10.3189/2015JoG15J015>, 2015.
- Isotta, F., Begert, M., and Frei, C.: Long-Term Consistent Monthly Temperature and Precipitation Grid Data Sets for Switzerland Over the Past 150 Years, *Journal of Geophysical Research: Atmospheres*, <https://doi.org/10.1029/2018JD029910>, 2019.
- 30 Isotta, F. A., Vogel, R., and Frei, C.: Evaluation of European regional reanalyses and downscalings for precipitation in the Alpine region, *Meteorologische Zeitschrift*, 24, 15–37, <https://doi.org/10.1127/metz/2014/0584>, 2014.
- Jennings, K. S., Winchell, T. S., Livneh, B., and Molotch, N. P.: Spatial variation of the rain – snow temperature threshold across the Northern Hemisphere, *Nature Communications*, <https://doi.org/10.1038/s41467-018-03629-7>, 2018.
- Johnson, J. B. and Schaefer, G. L.: The influence of thermal, hydrologic, and snow deformation mechanisms on snow water equivalent pressure sensor accuracy, *Hydrological Processes*, 16, 3529–3542, <https://doi.org/10.1002/hyp.1236>, 2002.
- 35 Jonas, T., Marty, C., and Magnusson, J.: Estimating the snow water equivalent from snow depth measurements in the Swiss Alps, *Journal of Hydrology*, 378, 161–167, <https://doi.org/10.1016/j.jhydrol.2009.09.021>, 2009.

- Jörg-Hess, S., Griessinger, N., and Zappa, M.: Probabilistic Forecasts of Snow Water Equivalent and Runoff in Mountainous Areas*, *Journal of Hydrometeorology*, 16, 2169–2186, <https://doi.org/10.1175/JHM-D-14-0193.1>, 2015.
- Kinar, N. J. and Pomeroy, J. W.: Measurement of the physical properties of the snowpack, *Reviews of Geophysics*, 53, 481–544, <https://doi.org/10.1002/2015RG000481>. Received, 2015.
- 5 Koch, F., Henkel, P., Appel, F., Schmid, L., Bach, H., Lamm, M., Prasch, M., Schweizer, J., and Mauser, W.: Retrieval of Snow Water Equivalent, Liquid Water Content, and Snow Height of Dry and Wet Snow by Combining GPS Signal Attenuation and Time Delay Water Resources Research, *Water Resources Research*, pp. 4465–4487, <https://doi.org/10.1029/2018WR024431>, 2019.
- Kochendorfer, J., Nitu, R., Wolff, M., Mekis, E., Rasmussen, R., Baker, B., Earle, M. E., Reverdin, A., Wong, K., Smith, C. D., Yang, D., Roulet, Y. A., Buisan, S., Laine, T., Lee, G., Aceituno, J. L. C., Alastrué, J., Isaksen, K., Meyers, T., Brækkan, R., Landolt, S., Jachcik, A., and Poikonen, A.: Analysis of single-Alter-shielded and unshielded measurements of mixed and solid precipitation from WMO-SPICE, *Hydrology and Earth System Sciences*, 21, 3525–3542, <https://doi.org/10.5194/hess-21-3525-2017>, 2017.
- 10 Kodama, M.: Continuous Monitoring of Snow Water Equivalent Using Cosmic-Ray Neutrons, *Cold Regions Science and Technology*, 3, 295–303, [https://doi.org/10.1016/0165-232X\(80\)90036-1](https://doi.org/10.1016/0165-232X(80)90036-1), 1980.
- Kodama, M., Kawasaki, S., and Wada, M.: A cosmic-ray snow gauge, *The International Journal Of Applied Radiation And Isotopes*, 26, 774–775, [https://doi.org/10.1016/0020-708X\(75\)90138-6](https://doi.org/10.1016/0020-708X(75)90138-6), 1975.
- 15 Kodama, M., Nakai, K., Kawasaki, S., and Wada, M.: An application of cosmic-ray neutron measurements to the determination of the snow-water equivalent, *Journal of Hydrology*, 41, 85–92, 1979.
- Lehning, M., Bartelt, P., Brown, B., Russi, T., Stöckli, U., and Zimmerli, M.: SNOWPACK model calculations for avalanche warning based upon a new network of weather and snow stations, *Cold Regions Science and Technology*, 30, 145–157, [https://doi.org/10.1016/S0165-232X\(99\)00022-1](https://doi.org/10.1016/S0165-232X(99)00022-1), 1999.
- 20 Lufft: Technical Data. VENTUS-UMB Ultrasonic Wind sensor, Tech. rep., Mess- und Regeltechnik GmbH, 2019.
- Martinaitis, S. M., Cocks, S. B., Qi, Y., Kaney, B. T., Zhang, J., and Howard, K.: Understanding Winter Precipitation Impacts on Automated Gauge Observations within a Real-Time System, *Journal of Hydrometeorology*, 16, 2345–2363, <https://doi.org/10.1175/JHM-D-15-0020.1>, 2015.
- 25 Marty, C., Abegg, B., Bauder, A., Marmy, A., Lüthi, M., Bavay, M., Hauck, C., Hoelzle, M., Huss, M., Salzmänn, N., Schlögl, S., Steiger, R., and Farinotti, D.: CH2014-Impacts. Toward quantitative scenarios of climate change impacts in Switzerland, chap. Cryospheric aspects of climate change - impacts on snow, ice and ski tourism, pp. 49–55, OCCR, FOEN, MeteoSwiss, C2SM, Agroscope, ProClim, 2014.
- MeteoSwiss: Documentation of MeteoSwiss Grid-Data Products Daily Precipitation (final analysis): RhiresD, Tech. Rep. August, <https://doi.org/OFEV2014>, <http://www.meteoschweiz.admin.ch/web/de/services/datenportal/gitterdaten/precip/rhiresd.Par.0007.DownloadFile.tmp/proddochhiresd.pdf>, 2013.
- 30 Mizukami, N. and Perica, S.: Spatiotemporal Characteristics of Snowpack Density in the Mountainous Regions of the Western United States, *Journal of Hydrometeorology*, 9, 1416–1426, <https://doi.org/10.1175/2008JHM981.1>, 2008.
- Papula, L.: *Mathematische Formelsammlung: für Ingenieure und Naturwissenschaftler*, Springer-Verlag, 2010, 10 edn., 2010.
- Paquet, E. and Laval, M.-t.: Experience feedback and future prospects for the use of EDF 's Cosmic-Ray Snow Gauges, *Société Hydrotechnique de France - Glaciology-Nivology Section*, p. 8, 2005.
- 35 Paquet, E., Laval, M.-t., Belov, A., Eroshenko, E., Kartyshev, V., Struminsky, A., and Yanke, V.: An application of cosmic-ray neutron measurements to the determination of the snow-water equivalent, in: 30th International Cosmic Ray Conference, vol. 1, pp. 761–764, [https://doi.org/10.1016/0022-1694\(79\)90107-0](https://doi.org/10.1016/0022-1694(79)90107-0), 2008.

- Pirazzini, R., Leppänen, L., Picard, G., Lopez-moreno, J. I., Marty, C., Macelloni, G., Kontu, A., von Lerber, A., Tanis, C. M., Schneebeli, M., de Rosnay, P., and Arslan, A. N.: European In-Situ Snow Measurements : Practices and Purposes, *Sensors*, 18, 2016 (51 pp.), <https://doi.org/10.3390/s18072016>, 2018.
- Pollock, M. D., O'Donnell, G., Quinn, P., Dutton, M., Black, A., Wilkinson, M. E., Colli, M., Stagnaro, M., Lanza, L. G., Lewis, E., Kilsby, C. G., and O'Connell, P. E.: Quantifying and Mitigating Wind-Induced Undercatch in Rainfall Measurements, *Water Resources Research*, 54, 3863–3875, <https://doi.org/10.1029/2017WR022421>, <https://agupubs.onlinelibrary.wiley.com/doi/abs/10.1029/2017WR022421>, 2018.
- Pulwiczki, A., Flowers, G. E., Radic, V., and Bingham, D.: Estimating winter balance and its uncertainty from direct measurements of snow depth and density on alpine glaciers, *Journal of Glaciology*, 64, 781–795, <https://doi.org/10.1017/jog.2018.68>, 2018.
- 10 Raleigh, M. S. and Small, E. E.: Snowpack density modeling is the primary source of uncertainty when mapping basin-wide SWE with lidar, *Geophysical Research Letters*, 44, 3700–3709, <https://doi.org/10.1002/2016GL071999>, 2017.
- Raleigh, M. S., Lundquist, J. D., and Clark, M. P.: Exploring the impact of forcing error characteristics on physically based snow simulations within a global sensitivity analysis framework, *Hydrology and Earth System Sciences*, 19, 3153–3179, <https://doi.org/10.5194/hess-19-3153-2015>, <https://www.hydrol-earth-syst-sci.net/19/3153/2015/>, 2015.
- 15 Rasmussen, R., Baker, B., Kochendorfer, J., Meyers, T., Landolt, S., Fischer, A. P., Black, J., Thériault, J. M., Kucera, P., Gochis, D., Smith, C., Nitu, R., Hall, M., Ikeda, K., and Gutmann, E.: How well are we measuring snow: The NOAA/FAA/NCAR winter precipitation test bed, *Bulletin of the American Meteorological Society*, 93, 811–829, <https://doi.org/10.1175/BAMS-D-11-00052.1>, 2012.
- Saito, K., Yamaguchi, S., Iwata, H., Harazono, Y., Kosugi, K., Lehning, M., and Shulski, M.: Climatic physical snowpack properties for large-scale modeling examined by observations and a physical model, *Polar Science*, 6, 79–95, <https://doi.org/10.1016/j.polar.2012.02.003>, 2012.
- 20 Schattan, P., Baroni, G., Oswald, S. E., Schöber, J., Fey, C., Kormann, C., Huttenlau, M., and Achleitner, S.: Continuous monitoring of snowpack dynamics in alpine terrain by aboveground neutron sensing, *Water Resources Research*, 53, 3615–3634, <https://doi.org/10.1002/2016WR020234>, 2017.
- Schmid, L., Heilig, A., Mitterer, C., Schweizer, J., Maurer, H., Okorn, R., and Eisen, O.: Continuous snowpack monitoring using upward-looking ground-penetrating radar technology, *Journal of Glaciology*, 60, 509–525, <https://doi.org/10.3189/2014JoG13J084>, 2014.
- 25 Schmid, L., Koch, F., Heilig, A., Prasch, M., Eisen, O., Mauser, W., and Schweizer, J.: A novel sensor combination (upGPR-GPS) to continuously and nondestructively derive snow cover properties, *Geophysical Research Letters*, pp. 3397–3405, <https://doi.org/10.1002/2015GL063732>, 2015.
- Schrön, M., Zacharias, S., Womack, G., Köhli, M., Desilets, D., Oswald, S. E., Bumberger, J., Mollenhauer, H., Kögler, S., Remmler, P., Kasner, M., Denk, A., and Dietrich, P.: Intercomparison of cosmic-ray neutron sensors and water balance monitoring in an urban environment, *Geoscientific Instrumentation, Methods and Data Systems*, 7, 83–99, <https://doi.org/10.5194/gi-7-83-2018>, 2018.
- 30 Sevruk, B., Ondrás, M., and Chvřla, B.: The WMO precipitation measurement intercomparisons, *Atmospheric Research*, 92, 376–380, <https://doi.org/10.1016/j.atmosres.2009.01.016>, 2009.
- Sigouin, M. J. P. and Si, B. C.: Calibration of a non-invasive cosmic-ray probe for wide area snow water equivalent measurement, *The Cryosphere*, 10, 1181–1190, <https://doi.org/10.5194/tc-2015-216>, 2016.
- 35 Sims, E. M. and Liu, G.: A parameterization of the orobability of snow–rain transition, *Journal of Hydrometeorology*, 16, 1466–1477, <https://doi.org/10.1175/jhm-d-14-0211.1>, 2015.

- SLF Data: Automatic snow stations from the Intercantonal Measurement and Information System (IMIS), WSL Institute for Snow and Avalanche Research SLF. Davos, Switzerland, 2015.
- Smith, T. and Bookhagen, B.: Assessing uncertainty and sensor biases in passive microwave data across High Mountain Asia, *Remote Sensing of Environment*, 181, 174 – 185, <https://doi.org/10.1016/j.rse.2016.03.037>, <http://www.sciencedirect.com/science/article/pii/S0034425716301419>, 2016.
- Smith, T. and Bookhagen, B.: Changes in seasonal snow water equivalent distribution in High Mountain Asia (1987 to 2009), *Science Advances*, 4, <https://doi.org/10.1126/sciadv.1701550>, <https://advances.sciencemag.org/content/4/1/e1701550>, 2018.
- Sold, L., Huss, M., Hoelzle, M., Anderegggen, H., Joerg, P. C., and Zemp, M.: Methodological approaches to infer end-of-winter snow distribution on alpine glaciers, *Journal of Glaciology*, 59, 1047–1059, <https://doi.org/10.3189/2013JoG13J015>, 2013.
- 10 Sold, L., Huss, M., Machguth, H., Joerg, P. C., Leysinger Vieli, G., Linsbauer, A., Salzmann, N., Zemp, M., and Hoelzle, M.: Mass Balance Re-analysis of Findelengletscher, Switzerland; Benefits of Extensive Snow Accumulation Measurements, *Frontiers in Earth Science*, 4, 18, <https://doi.org/10.3389/feart.2016.00018>, <https://www.frontiersin.org/article/10.3389/feart.2016.00018>, 2016.
- Sorteberg, H. K., Engeset, R. V., and Udnæs, H. C.: A national network for snow monitoring in Norway: Snow pillow verification using observations and models, *Physics and Chemistry of the Earth, Part C: Solar, Terrestrial and Planetary Science*, 26, 723–729, [https://doi.org/10.1016/S1464-1917\(01\)95016-0](https://doi.org/10.1016/S1464-1917(01)95016-0), 2001.
- 15 Steiner, L., Meindl, M., Fierz, C., and Geiger, A.: An assessment of sub-snow GPS for quantification of snow water equivalent, *The Cryosphere*, 12, 3161–3175, <https://doi.org/10.5194/tc-12-3161-2018>, 2018.
- Steiner, L., Meindl, M., Marty, C., and Geiger, A.: Impact of GPS Processing on the Estimation of Snow Water Equivalent Using Refracted GPS Signals, *IEEE Transactions on Geoscience and Remote Sensing*, pp. 1–13, <https://doi.org/10.1109/TGRS.2019.2934016>, 2019.
- 20 Stuefer, S., Kane, L. D., and Liston, G. E.: In situ snow water equivalent observations in the U . S . Arctic, *Hydrology Research*, 44, 21–34, <https://doi.org/10.2166/nh.2012.177>, 2013.
- Sturm, M., Taras, B., Liston, G. E., Derksen, C., Jonas, T., and Lea, J.: Estimating Snow Water Equivalent Using Snow Depth Data and Climate Classes, *Journal of Hydrometeorology*, 11, 1380–1394, <https://doi.org/10.1175/2010JHM1202.1>, 2010.
- Sturm, M., Goldstein, M. A., and Parr, C.: Water and life from snow: A trillion dollar science question, *Water Resources Research*, pp. 3534–3544, <https://doi.org/10.1002/2017WR020840>.Received, 2017.
- 25 Thibert, E., Blanc, R., Vincent, C., and Eckert, N.: Glaciological and volumetric mass-balance measurements: Error analysis over 51 years for Glacier de Sarennes, French Alps, *Journal of Glaciology*, 54, 522–532, <https://doi.org/10.3189/002214308785837093>, 2008.
- Vionnet, V., Brun, E., Morin, S., Boone, A., Faroux, S., Le Moigne, P., Martin, E., and Willemet, J.-M.: The detailed snowpack scheme Crocus and its implementation in SURFEX v7.2, *Geoscientific Model Development*, 5, 773–791, <https://doi.org/10.5194/gmd-5-773-2012>, <https://www.geosci-model-dev.net/5/773/2012/>, 2012.
- 30 Viviroli, D., Dürr, H. H., Messerli, B., Meybeck, M., and Weingartner, R.: Mountains of the world, water towers for humanity: Typology, mapping, and global significance, *Water Resources Research*, 43, W07 447, <https://doi.org/10.1029/2006WR005653>, 2007.
- Viviroli, D., Archer, D. R., Buytaert, W., Fowler, H. J., Greenwood, G. B., Hamlet, A. F., Huang, Y., Koboltschnig, G., Litaor, M. I., López-Moreno, J. I., Lorentz, S., Schädler, B., Schreier, H., Schwaiger, K., Vuille, M., and Woods, R.: Climate change and mountain water resources: Overview and recommendations for research, management and policy, *Hydrology and Earth System Sciences*, 15, 471–504, <https://doi.org/10.5194/hess-15-471-2011>, 2011.
- 35 Zreda, M., Desilets, D., Ferré, T. P. A., and Scott, R. L.: Measuring soil moisture content non-invasively at intermediate spatial scale using cosmic-ray neutrons, *Geophysical Research Letters*, 35, <https://doi.org/10.1029/2008GL035655>, 2008.

Zreda, M., Shuttleworth, W. J., Zeng, X., Zweck, C., Desilets, D., Franz, T., and Rosolem, R.: COSMOS: The cosmic-ray soil moisture observing system, *Hydrology and Earth System Sciences*, 16, 4079–4099, <https://doi.org/10.5194/hess-16-4079-2012>, 2012.